TU Delft

Delft University of Technology

Document Version
Final published version

Licence
Dutch Copyright Act (Article 25fa)

Citation (APA)
Aleo, A., Bradtmöller, M., Chasan, R., Despotopoulou, M., Fernández, L. G., Gomez, J. A. G., Kozowyk, P. R. B., Rodríguez, F., & Langejans, G. H. J. (2026). The Needle in the Haystack: a Multi-Analytical Approach for the Identification of Palaeolithic Adhesive Residues at Morín Cave, Spain. *Journal of Paleolithic Archaeology*, *9*(1), Article 2. https://doi.org/10.1007/s41982-025-00251-0

Important note
To cite this publication, please use the final published version (if applicable).
Please check the document version above.

Copyright
In case the licence states “Dutch Copyright Act (Article 25fa)”, this publication was made available Green Open Access via the TU Delft Institutional Repository pursuant to Dutch Copyright Act (Article 25fa, the Taverne amendment). This provision does not affect copyright ownership.
Unless copyright is transferred by contract or statute, it remains with the copyright holder.

Sharing and reuse
Other than for strictly personal use, it is not permitted to download, forward or distribute the text or part of it, without the consent of the author(s) and/or copyright holder(s), unless the work is under an open content license such as Creative Commons.

Takedown policy
Please contact us and provide details if you believe this document breaches copyrights.
We will remove access to the work immediately and investigate your claim.

This work is downloaded from Delft University of Technology.

Journal of Paleolithic Archaeology (2026) 9:2
https://doi.org/10.1007/s41982-025-00251-0

RESEARCH

The Needle in the Haystack: a Multi-Analytical Approach for the Identification of Palaeolithic Adhesive Residues at Morín Cave, Spain

Alessandro Aleo[1,2] · Marcel Bradtmöller[3] · Rivka Chasan[1] · Myrto Despotopoulou[1] · Luis Gómez Fernández[4] · Jesus Antonio Gonzalez Gomez[4] · Paul R. B. Kozowyk[1] · Fernando Rodríguez[4] · Geeske H. J. Langejans[1,5]

Received: 20 March 2024 / Accepted: 8 December 2025
© The Author(s), under exclusive licence to Springer Nature Switzerland AG 2025

Abstract
Adhesives are central to debates on the cognitive and technological capabilities of Neanderthals and modern humans. Spectrometric and chemical analyses suggest that Neanderthals relied primarily on birch bark tar, with some use of bitumen and conifer resin, whereas modern humans employed a broader range of materials, including resins, gums, tars, beeswax, and bitumen, sometimes mixed with inorganic additives. This evidence reveals a complex and varied technological landscape in which adhesive recipes were shaped by raw material availability, functional requirements, and cultural traditions. To explore Palaeolithic adhesive technology, we applied a multi-analytical approach—including optical and scanning electron microscopy, spectrometry, and chemical analyses—to lithic assemblages spanning the entire sequence of Morín Cave, northern Spain. This integrated protocol enabled us to distinguish modern contaminants from residues of probable archaeological origin and to suggest the presence of adhesives on a Châtelperronian and a Gravettian tool. Gas chromatography–mass spectrometry (GC-MS) detected resin or tar from a *Cupressaceae* plant on the Châtelperronian point, while potential insect wax, plant wax, or bitumen was identified on the Gravettian tool. Together with earlier observations of possible adhesive residues at Morín (Bradtmöller et al., *Journal of Archaeological Science*, 7:1-13, 2016), these findings increase the number of chemically supported cases to four, making the site one of the few in Europe with potential adhesive evidence spanning multiple Palaeolithic technocomplexes. The residues are consistent with hafting applications, likely linked to projectile technology, though the degree of certainty varies. Although the limited number of identified residues and difficulties in precise characterisation prevent direct comparison of Neanderthal and modern human adhesive traditions at Morín Cave, our results provide insights into Palaeolithic adhesive use. More importantly, they demonstrate the potential of a multi-analytical methodology to disentangle ancient residues from modern contaminants and to advance the systematic study of prehistoric adhesive technologies.

Keywords Adhesives · Traceology · Spectroscopy · GC-MS · Ochre · Palaeolithic

✉ Alessandro Aleo
alealeo89@gmail.com

[1] Department of Materials Science and Engineering, Faculty of Mechanical Engineering, Delft University of Technology, Delft 2628 CD, the Netherlands

[2] Department of Archaeological Sciences, Faculty of Archaeology, Leiden University, Leiden 2333 CC, the Netherlands

[3] Heinrich Schliemann-Institute for Ancient Studies, Rostock University, Rostock 18055, Germany

[4] Department of Earth Sciences and Condensed Matter Physics, Faculty of Sciences, University of Cantabria, Santander 39005, Spain

[5] Palaeo-Research Institute, University of Johannesburg, Johannesburg 2092, South Africa

Introduction

In the last decades, prehistoric adhesives have attracted increasing scientific attention. Due to the age of this technology (Mazza et al., 2006) and the cognitive processes and skills it requires (Wadley et al., 2009; Wragg Sykes, 2015), adhesives are a key component in debates about Neanderthal and anatomically modern human (AMH) technological and cognitive complexity (Fajardo et al., 2023; Kozowyk et al., 2023; Roebroeks & Soressi, 2016; Schmidt et al., 2023). Pleistocene adhesives from European Palaeolithic sites are rare in the archaeological record. Being organic materials, they generally preserve poorly, yet they are attested in several assemblages across Eurasia.

Published online: 03 January 2026

In western and central Europe, Middle Palaeolithic adhesives associated with Neanderthals and identified chemically (Table 1) consist almost exclusively of birch bark tar (Koller et al., 2001; Mazza et al., 2006; Niekus et al., 2019). Exceptions are the adhesives from Fosellone and Sant'Agostino Caves (Italy), where conifer resin and occasionally a mixture of resin and beeswax were used (Degano et al., 2019). In eastern Europe and the Levant, natural bitumen was exploited, likely by Neandertals, as hafting adhesives as identified at Mezmaiskaya Cave and Saradj-Chuko Grotto (Russia), Gura Cheii-Râşnov Cave (Romania), Umm el Tlel, and Hummal (Syria) (Boëda et al., 2008b; Cârciumaru et al., 2012; Doronicheva et al., 2022; Hauck et al., 2013). The bitumen residues at Umm el Tlel and Hummal are associated with Mousterian industries, traditionally attributed to Neanderthals. However, given the early and recurrent presence of AMH in southwest Asia (Hershkovitz et al., 2018), and the documentation of AMH as Mousterian makers in the Levant (Zaidner & Weinstein-Evron, 2020), an exclusive attribution of these residues to Neanderthals cannot be sustained with certainty. A possible goethite-loaded bitumen adhesive (Schmidt et al., 2024) was also recently identified at Le Moustier (France) (but see Rots et al., 2024 for a counter-argument). The Levallois association links this evidence to the Mousterian technocomplex, but as it derives from early 20th-century excavations and lacks direct radiometric dating, its taxonomic and chronological attribution is uncertain.

The limited evidence for Upper Palaeolithic adhesives identified through chemical and spectroscopic analyses (Table 1) suggests that AMH exploited a slightly broader

Table 1 Chemically and spectrometrically identified adhesives from European Pleistocene. *Traditionally attributed to Neanderthal but attribution is not exclusive

Site	Age	Attribution	Adhesive	Additives	Tool type	Methods	Reference
Campitello Quarry (IT)	>190 ka	Neanderthal (chronostratigraphy)	Birch bark tar	-	2 flakes	SEM-EDX, FTIR, GC-MS	(Mazza et al., 2006)
Saradj-Chuko Grotto (RU)	92–41 ka	Neanderthal (Mousterian technocomplex)	Bitumen	-	1 side-scraper 1 point 2 convergent scrapers	SEM-EDX, FTIR, Raman	(Doronicheva et al., 2022)
Hummal (SY)*	80–50 ka	Neanderthal (association with Tabun B-type Mousterian)	Bitumen	-	1 Levallois points 1 Mousterian point 1 Levallois flake	SEM-EDX, FTIR, confocal Raman, GC-MS	(Hauck et al., 2013; Monnier et al., 2013)
Umm el Tlel (SY)*	~71 ka	Neanderthal (stratigraphic position and association with Mousterian industry)	Bitumen	-	11 Levallois artefacts	GC-MS	(Boëda et al., 2008a, b)
Mezmaiskaya Cave (RU)	~70–40 ka	Neanderthal (Mousterian technocomplex)	Bitumen	-	1 convergent scraper	SEM-EDX, FTIR, Raman	(Doronicheva et al., 2022)
Le Moustier (FR)*	56–40 ka	Neanderthal (Mousterian industry. No radiometric dates available)	Bitumen	Goethite	1 end-notched flake 1 retouched Levallois blade	SEM-EDX, ATR-FTIR, Raman	(Schmidt et al., 2024)
Fosellone Cave (IT)	55–40 ka	Neanderthal (from level 23α with typical Mousterian industry)	Conifer resin	Beeswax	3 scrapers 1 flake	GC-MS	(Degano et al., 2019)
Zandmotor beach (NL)	~50 ka (direct dating)	Neanderthal	Birch bark tar	-	1 flake	THM-Py-GC/MS	(Niekus et al., 2019)
Königsaue (DE)	>43 ka and >48 ka (direct dating)	Neanderthal (association with Mousterian industry)	Birch bark tar	-	Free lumps	GC-MS	(Koller et al., 2001)
Sant'Agostino Cave (IT)	~43 ka	Neanderthal (Mousterian industry)	Conifer resin	-	5 scrapers 1 Levallois flake	GC-MS	(Degano et al., 2019)
Gura Cheii-Râşnov Cave (RO)	Undefined Mousterian	Neanderthal	Bitumen	-	1 retouched flake	FTIR, EDXRF, GC-MS, ICP-AES	(Cârciumaru et al., 2012)
Grotta del Cavallo (IT)	~45–39 ka	AMH (Uluzzian technocomplex)	Plant/tree gum	Beeswax Ochre	6 backed points	SEM-EDX, FTIR	(Sano et al., 2019)
Morín Cave (ES)	>36.5 ka and ~24 ka	AMH (Aurignacian and Gravettian technocomplexes)	Natural resin/proteinaceous material	Ochre Possibly burnt bone	1 backed blade 1 partially backed blade 1 burin 1 truncation	SEM-EDX, FTIR, Raman	(Bradtmöller et al., 2016)
Hinxton (UK)	~15–12 ka cal BP	AMH	Conifer tar, maybe resin	-	1 backed blade	THM-Py-GC-MS	(Langejans et al., 2023)
Bergkamen (DE)	~13 ka (direct dating)	AMH	Beeswax	-	1 barbed point	FTIR, Py-GC-MS	(Baales et al., 2017)
Maasvlakte 2 (NL)	~13 ka cal BP (direct dating)	AMH	Birch bark tar	-	1 barbed point	GC-MS	(Aleo et al., 2023)
Gura Cheii-Râşnov Cave (RO)	Undefined Upper Palaeolithic	AMH	Bitumen	-	1 backed blade	FTIR, EDXRF, GC-MS, ICP-AES	(Cârciumaru et al., 2012)

range of materials than Neanderthals. These included birch and conifer tar, resin, beeswax, bitumen, iron oxides, and possibly burnt bone as additives (Aleo et al., 2023; Baales et al., 2017; Bradtmöller et al., 2016; Cârciumaru et al., 2012; Sano et al., 2019). Ochre has been documented in a few Upper Palaeolithic adhesive mixtures (Bradtmöller et al., 2016; Sano et al., 2019), and its use is well-known in Middle and Later Stone Age African adhesive technology (e.g., Gibson et al., 2004; Lombard, 2006; Rots et al., 2011). Conversely, although there is evidence for the use of different iron oxides by Neandertals (e.g., Dayet et al., 2014; Dayet et al., 2019; Roebroeks et al., 2012), direct evidence for the use of ochre as an adhesive component is extremely limited, with only a single instance reported, whose attribution to Neanderthals remains uncertain (Schmidt et al., 2024) as does its chemical characterisation (Rots et al., 2024).

Taken together, the available data reveal a complex and varied picture of adhesive technologies among Neanderthals and AMH. Molecular analyses demonstrate that prehistoric adhesives were manufactured from diverse natural sources, including tree resins and gums, plant and insect waxes, bark and wood tars, and bitumen. The choice of raw materials appears to have depended on environmental availability, intended function, technological knowledge, and working properties, and may also reflect cultural traditions. Nothing can be said about differences in production methods during the Palaeolithic since it is yet unknown how adhesives were produced although some methods have been proposed (Kozowyk et al., 2017; Schmidt et al., 2019, 2023). Yet, despite their central role in the current debate on ancient human behaviour and technology, the actual use and reuse of prehistoric adhesives is understudied. Our understanding of past adhesive technology suffers from the lack of a systematic application of multi-analytical methods for adhesive characterisation, specifically on large samples.

To address these issues and further investigate Palaeolithic adhesive technology, we analysed the lithic assemblage from Morín Cave in northern Iberia (Fig. 1). The collection was considered particularly promising for two reasons. First, Bradtmöller et al. (2016) reported possible adhesive residues on a few Upper Palaeolithic tools from Morín and noted similar traces in other stratigraphic units, suggesting that the assemblage merited further analysis. Second, the site preserves an exceptional stratigraphic sequence spanning from the Middle to the end of the Upper Palaeolithic, encompassing both Neanderthal and AMH occupations.

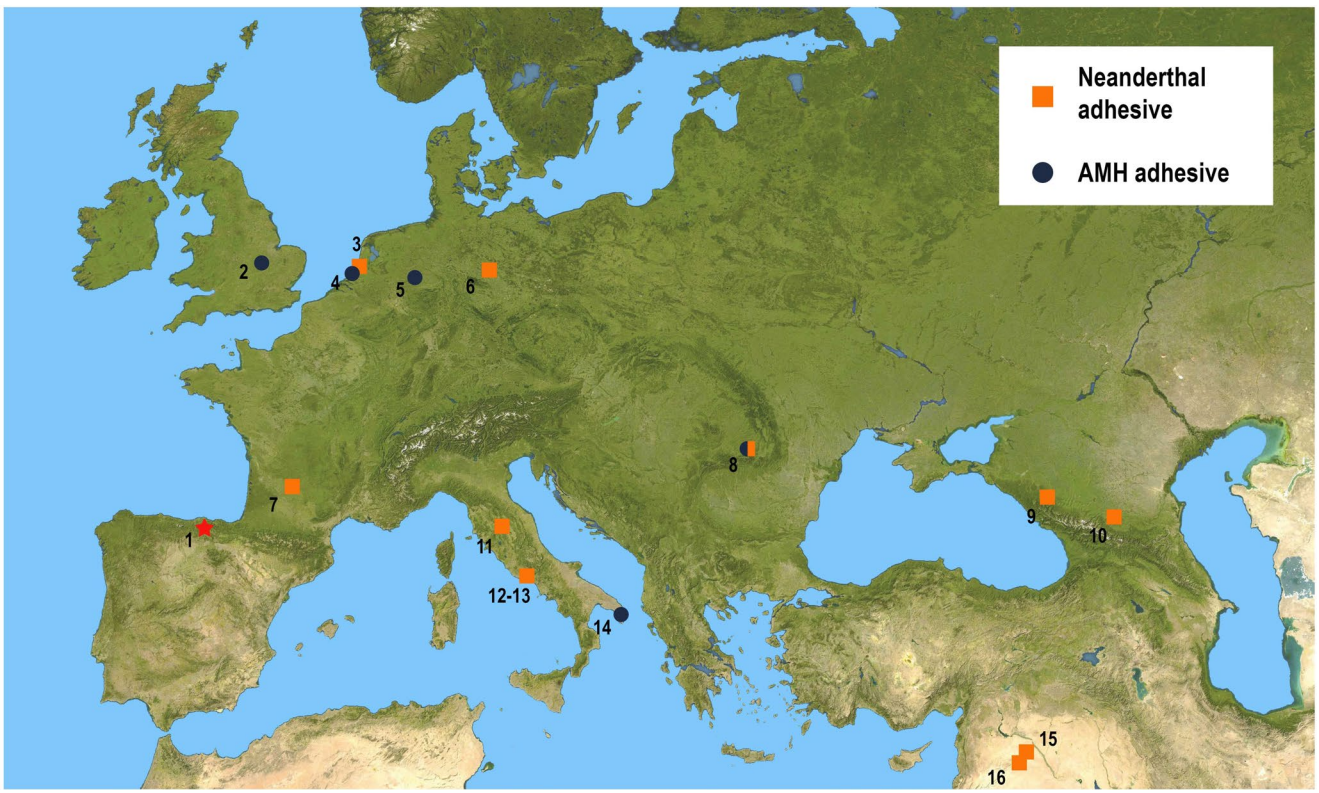


Fig. 1 Distribution of spectrochemically identified Eurasian prehistoric adhesives. (1) Morín Cave (ES); (2) Hinxton (UK); (3) Zandmotor (NL); (4) Maasvlakte 2 (NL); (5) Bergkamen (DE); (6) Königsaue (DE); (7) Le Moustier (FR); (8) Gura Cheii-Râşnov Cave (RO); (9) Mezmaiskaya Cave (RU); (10) Saradj-Chuko Grotto (RU); 11) Campitello Quarry (IT); 12) Fosellone Cave (IT); 13) Sant'Agostino Cave (IT); 14) Grotta del Cavallo (IT); 15) Hummal (SY); 16) Umm el Tlel (SY). Base map via Pixabay

This allows for detailed discussion of adhesive variability and versatility in relation to tool function, material properties, natural resource use, diachronic technological developments, and intra-group comparisons. Furthermore, many key sites of this region have been recently reviewed and redated providing a chronological and environmental framework in which the results of the analysis of Morín Cave can be contextualised (Fernández-García et al., 2023; Jones et al., 2019; Marín-Arroyo et al., 2018).

In this study, we applied a holistic, multi-step methodology that combines microscopic use-wear and residue analysis with chemical and spectrometric techniques for residue characterisation. Through this integrated approach, we aim not only to expand our understanding of Neanderthal and AMH adhesive traditions but also to demonstrate the value of multi-analytical strategies for the systematic investigation of Palaeolithic adhesive residues.

Materials and Methods

The Site and Studied Assemblage

Morín Cave is located in Villanueva de Villaescusa (Cantabria), 6 km off the modern coastline. The cave was discovered in the early 1900s, and several excavation campaigns have since taken place (Carballo, 1923; Echegaray et al., 1971; Obermaier, 1916). The main archaeological exploration was between 1966 and 1969, when a long stratigraphy consisting of 22 layers was exposed. The sequence includes one Azilian (layer 1), one Magdalenian (layer 2), one Solutrean (layer 3), two Gravettian (layers 4 and 5b), one evolved and two early Aurignacian (layers 5a, 6, and 7), two Protoaurignacian (layers 8 and 9), one Châtelperronian (layer 10), and eight Mousterian (layers 11–17 and 22) layers (Maíllo-Fernández et al., 2014).

The chrono-cultural sequence is mostly based on the lithic assemblage, as several dating attempts provided unsatisfactory results (Maíllo-Fernández et al., 2014; Marín-Arroyo et al., 2018). Several authors have raised concerns about the stratigraphic integrity of the Morín sequence, especially regarding the Middle-to-Upper Palaeolithic transition layers. In particular, the accumulation of material in layer 10, attributed to the Châtelperronian, may have resulted from the movement of artifacts between layers due to the admixture of Mousterian, Châtelperronian, and Aurignacian elements or to depositional processes, e.g., solifluction, erosion, and cryoturbation, at the interface between layer 11 (Mousterian) and layer 9 (Protoaurignacian) (Sanguino et al., 2005; Zilhao, 2006). Such movement may explain the inconsistent dates for layers 10 and 9 obtained in the years. On the contrary, other authors (Arrizabalaga & Iriarte, 2006; Maíllo-Fernández et al., 2014) after having reassessed the site stratigraphy and lithic collection, argued that the Châtelperronian at Morín is a well-defined cultural complex that differs from the preceding and following cultural units. The lithic production is oriented toward the production of blades, and more marginally bladelets, from unipolar and bipolar cores. These are then transformed into typical Châtelperronian points (Maíllo-Fernández, 2005). In the overlaying Protoaurignacian layers (layers 9 and 8), tentatively dated at ~36.6 ka BP (Maíllo-Fernández et al., 2001), bladelets and blades are produced in a continuum from prismatic unipolar cores and they are the goal of the production. The former are almost exclusively transformed into Dufour bladelets (Maíllo-Fernández, 2006). Tools manufactured on flakes, such as side scrapers, denticulates, and notches, and flake technology using knapping methods with a discoidal concept also play a significant role in these layers (Maíllo-Fernández, 2012). The Early Aurignacian (layers 6 and 7) is characterised by the high frequency of carinated pieces and two different laminar reduction methods: blades are produced from prismatic unipolar cores while bladelets are produced from carinated cores (Cabrera et al., 2004).

In 2016, Bradtmöller and colleagues reported the presence of potential adhesive remains on three Gravettian and one Aurignacian tools (Bradtmöller et al., 2016). The residues were analysed using scanning electron microscopy-energy-dispersive X-ray spectrometry (SEM-EDX), Fourier transform infrared spectroscopy (FTIR), and Raman spectroscopy and interpreted as adhesives made of natural resin mixed with ochre and possibly burnt bones (Bradtmöller et al., 2016). With the aim of chemically characterising these residues and identifying more adhesives, we inspected the entire lithic collection of Morín Cave (N=23,796), covering the entire stratigraphic sequence of the cave.

The material is stored and curated at the Museo de Prehistoria y Arqueología de Cantabria (MUPAC), Santander (ES). Post excavation, the collection has been extensively handled and studied. The tools were handled, analysed for typology and technology, photographed, drawn, labelled, and numbered. All of these actions resulted in some macro- and microscopic traces on the objects, i.e., pencil marks, ink, clear varnish, and modelling clay, potentially contaminating ancient wear traces and residues (Pedergnana et al., 2016). Other potential contaminations, such as skin flakes and lipids from handling are more subtle and harder to be visually detected and removed during cleaning thus requiring careful consideration (cf. Frahm et al., 2022; Pedergnana et al., 2016). Additionally, the tools were stored in plastic bags; therefore, contamination from storage may also have occurred (Frahm et al., 2022).

All the lithic tools with at least one usable edge were macroscopically analysed with a stereo microscope to detect

potential adhesive residues. We excluded tools with unknown stratigraphic position or from mixed layers, blocks, cores, and Mousterian material smaller than 1 cm. After this first examination, we selected 62 tools with ochre stains, discolouration, or black/brownish adhering residues for a more detailed investigation using a metallographic microscope. Then, we selected 31 tools with potential adhesives based on the location, distribution, appearance, and surface quality of the residues. Three of the four tools with adhesive remains already identified in 2016 were reanalysed for use-wear and GC-MS (MOR1, MOR5, and MOR6). To avoid further contamination of the tools, after their selection, the tools were gently washed with water and neutral soap and handled using powder-free nitrile gloves. Despite that, previous experimental work showed that it is almost impossible to eliminate modern contamination from archaeological tools completely (Hayes & Rots, 2019; Pedergnana et al., 2016).

The residue on the selected tools can be divided into two groups: residue spots < 1 mm, barely visible without a stereomicroscope and thus too small to be sampled for chemical analysis ($N = 12$), and those larger and thicker than 1 mm, large enough to be sampled with a scalpel blade or cotton swab ($N = 19$). The former, excluding MOR6, were analysed with SEM-EDX and micro-Raman to confirm their organic nature and gain insights into their molecular structure; the latter were analysed with GC-MS for their molecular characterisation (Table 2). All residues in the proximity of visible modern sources of contamination, such as ink and clear varnish, were not sampled or measured. Additionally, samples of sediments were taken from each archaeological layer to serve as control samples for contaminations. Among them, three samples were analysed with ATR-FTIR and GC-MS to rule-out sediment contamination (Table 2). The sediment samples were collected either from poorly washed tools from which residues were sampled or from sediment samples available in the collection.

We excluded 31 tools selected after examination with the stereomicroscope because the residues were randomly distributed on the surfaces or were identified as mineral deposits and manganese oxide stains with high power microscopy. Black manganese oxide deposits appear as diffuse spots or dendritic patterns (Randolph-Quinney et al., 2016). To verify the accuracy of our interpretation of mineral deposits based on optical microscopy, we selected four tools with manganese oxide/post-depositional stains for GC-MS analysis. Therefore, the final number of analysed tools is 35 (Table 2).

The studied assemblage consists mostly of complete and fragmented blades and bladelets, some of which are retouched, as well as points, with a total of 24 artifacts (Table 2). These tool types are often assumed to have been used as projectiles or elements of composite tools that were hafted. Thus, the staining on these tools can potentially represent adhesive remains used to attach them to the haft. However, the sample also features so-called 'domestic tool types' (N = 11), such as endscrapers and retouched flakes (Table 2), for which hafting it is not an absolute precondition and may be therefore overlooked.

Methods of Analysis

The tools and their residues were analysed with a multi-analytical approach including optical and scanning electron microscopy, spectrometry (ATR-FTIR and micro-Raman), and chemical analysis (GC-MS).

Optical Microscopy

Use-wear traces and residues were studied through optical microscopy following established protocols (Coppe & Rots, 2017; Fullagar, 2006; Langejans & Lombard, 2015; Van Gijn, 2010). We employed a Leica M80 stereomicroscope (magnification 7.5x-60x) for documenting the presence of residues on the surfaces of tools and mapping their distribution and for macro-wear analysis (low-power approach, Semenov, 1964; Tringham et al., 1974). A Leica DM2500 M metallographic microscope (magnification 50x-500x) was employed for the morphological description of residues and micro-wear analysis (high-power approach, Keeley, 1980). Pictures of wear traces and residues were taken using a Leica DFC425 C digital camera. Photos of archaeological use-wear traces and residues were compared with experimental traces and residues on the reference collection of the Laboratory for Material Cultural Studies (Leiden University, NL) which includes more than 4000 experiments. As the analysis did not take place where the collection is housed, photo-based comparison was used as a necessary alternative. Additionally, high resolution casts of representative use-wear traces were taken using vinylpolysiloxane precision impression material manufactured by Provil novo.

Microscopic Residues (< 1 mm)

Eleven tools displaying microscopic residues were analysed with scanning electron microscopy-energy dispersive X-ray spectrometry (SEM-EDX) to provide elemental information allowing the verification of the organic nature of the residues (Table 2). A scanning electron microscope (VPSEM) ZEISS EVO MA15 with an integrated EDX system was used for the analysis. We have worked in variable pressure, accelerating voltage 15 keV, and working distance between 8.5 and 9.5 mm. We measured at least two residue spots for each archaeological tool, and for tools with residues displaying

Table 2 Overview of the tools with potential adhesive remains and the analyses performed. *Analyses performed by Bradtmöller et al. (2016). Tools with two asterisks (**) display mineral/manganese deposits

ID	Layer	Cultural affiliation	Tool type	Residue location	Analyses
MOR1/ Artefact B	9	Protoaurignacian	Retouched blade (proximal-mesial fragment)	Dorsal and ventral face	Microscopy, GC-MS, SEM-EDX, micro-Raman*
MOR2	9	Protoaurignacian	Endscraper	Dorsal and ventral	Microscopy, SEM-EDX, micro-Raman
MOR4	7	Early Aurignacian	Dufour bladelet (proximal fragment)	Dorsal, ventral, back	Microscopy, SEM-EDX, micro-Raman
MOR5/ Artefact C	5a	Gravettian	Truncation	Dorsal, ventral, back	Microscopy, GC-MS, SEM-EDX, micro-Raman*
MOR6/ Artefact A	4	Gravettian	Retouched blade (proximal fragment)	Dordal and ventral	Microscopy. Most of the residue removed in 2016, SEM-EDX, micro-Raman, FTIR*
MOR9	10	Châtelperronian	Châtelperronian point	Dorsal, ventral, back	Microscopy, SEM-EDX, micro-Raman
MOR11	10	Châtelperronian	Backed point (atypical Châtelperronian point)	Dorsal, ventral, back	Microscopy, ATR-FTIR, GC-MS
MOR12	5a	Gravettian	Truncation	Back and dorsal	Microscopy, SEM-EDX
MOR13	6	Early Aurignacian	Backed blade (proximal fragment)	Dorsal, ventral, back	Microscopy, SEM-EDX, micro-Raman
MOR14	5a	Gravettian	Backed bladelet	Dorsal, ventral, back	Microscopy, GC-MS
MOR17	9	Protoaurignacian	Endscraper	Dorsal and ventral	Microscopy, SEM-EDX
MOR22	Trench 9	Upper Palaeolithic	Blade (proximal-mesial fragment)	Ventral	Microscopy, SEM-EDX, micro-Raman
MOR24	10	Châtelperronian	Blade (proximal fragment)	Dorsal and ventral	Microscopy, GC-MS
MOR25	10	Châtelperronian	Bladelet (natural back)	Dorsal, ventral, back	Microscopy, GC-MS
MOR28	10	Châtelperronian	Blade (mesial fragment)	Dorsal and ventral	Microscopy, GC-MS
MOR32	7	Early Aurignacian	Endscraper	Dorsal and ventral	Microscopy, GC-MS
MOR35	2	Magdalenian	Backed blade (mesial fragment)	Dorsal, ventral, back	Microscopy, SEM-EDX
MOR40	8a	Protoaurignacian	Blade (mesial fragment)	Dorsal and ventral	Microscopy, ATR-FTIR, GC-MS
MOR41	10?	Châtelperronian	Flake (natural back)	Dorsal, ventral, back	Microscopy, GC-MS
MOR42	9	Protoaurignacian	Retouched flake	Dorsal	Microscopy, SEM-EDX
MOR43	10	Châtelperronian	Blade (mesial fragment)	Dorsal and ventral	Microscopy, ATR-FTIR, GC-MS
MOR45	7	Early Aurignacian	Flake (natural back)	Dorsal and ventral proximal	Microscopy, GC-MS
MOR47	8	Protoaurignacian	Endscraper	Dorsal and ventral	Microscopy, ATR-FTIR, GC-MS
MOR49	8	Protoaurignacian	Bladelet with convergent edges	Dorsal	Microscopy, GC-MS
MOR50	8	Protoaurignacian	Bladelet (mesial-distal fragment)	Dorsal and ventral	Microscopy, SEM-EDX
MOR57	13	Mousterian	Flake	Ventral left edge	Microscopy, GC-MS
MOR58	13	Mousterian	Laminar flake (distal-mesial fragment)	Ventral, dorsal right edge	Microscopy, GC-MS
MOR59	16	Mousterian	Levallois point	Ventral	Microscopy, SEM-EDX, micro-Raman
MOR60	16	Mousterian	Discoid point	Dorsal and ventral	Microscopy, GC-MS
MOR61	Aurignacian	Aurignacian	Retouched flake	Dorsal	Microscopy, GC-MS
MOR62	1	Azilian	Bladelet (mesial fragment)	Dorsal	Microscopy, GC-MS
MOR26**	10	Châtelperronian	Blade (fragment)	Dorsal and ventral	Microscopy, GC-MS
MOR38**	8a	Protoaurignacian	Flake	Dorsal	Microscopy, ATR-FTIR, GC-MS
MOR44**	10	Châtelperronian	Flake	Dorsal (mostly) and ventral	Microscopy, ATR-FTIR, GC-MS
MOR46**	8	Protoaurignacian	Blade (fragment)	Dorsal and ventral	Microscopy, ATR-FTIR, GC-MS
SED1	5	Gravettian	Sediment	/	GC-MS
SED2	8	Protoaurignacian	Sediment	/	ATR-FTIR
SED3	10	Châtelperronian	Sediment	/	ATR-FTIR, GC-MS

a strong carbon (C) peak, a measurement of the rock substrate was also collected to cross-check the results. Based on the results of SEM-EDX, five tools bearing potential organic residues and one with mineral deposits were further analysed with micro-Raman (Table 2). The Raman analysis also included five experimentally recreated adhesives, namely pine tar, birch bark tar, pine resin, beeswax, pine resin + beeswax, and pine resin + beeswax + ochre, to serve as reference collection. We carried out in situ Raman analysis using a BWTEK Raman device, composed an MGL-III-532-100mW CF61800 green laser (532 nm) and an FCD785 laser (785 nm), with an BWTEK BAC100-785E Raman head, and two BWTEK GLACIER X BTC112E spectrometers with a Hamamatsu CCD detector (S10141-1107 S; 2048 pixels). The equipment covers a wavenumber range in Raman displacement of 80–3600 cm^{-1}, with a spectral resolution of 4 cm^{-1} measured as FWHM. Spectra were acquired using commercial software provided by BWTEK. The maximum laser power was 10 mW on the sample surface to prevent thermal degradation of the materials, which is normally evidenced by a drastic increase in the Raman spectrum background. The mean integration time ranged from 2 to 60 s, and 5 accumulations were performed in each run. The confocal Raman microscope is equipped with 20x and 50x objectives and a CCD camera for imaging that allow us to select the focus point of the excitation laser probe on the sample.

Macroscopic Residues (> 1 mm)

Twenty-three tools displaying macroscopic residues, including 19 with potential adhesive remains and four with mineral deposits identified through optical microscopy, were sampled for molecular analysis (Table 2). The latter were included to validate our interpretation of residue as inorganic based on the morphology. Residue samples were removed from each object with a sterile scalpel blade ($N=15$), with a cleaned cotton swab dipped in methanol ($N=8$), or by submerging the tool in methanol and sonicating for 20 min at 30˚C ($N=1$). The residue on MOR38 was sampled using both a scalpel blade and a cotton swab to compare results of the two extraction methods. From these, we randomly selected seven residue samples for attenuated total reflectance (ATR) analysis (Table 2) to verify the results. For the ATR analysis, we used a Perkin Elmer Spectrum 100 FT-IR Spectrometer with a diamond crystal. The software for equipment control and data evaluation was the Spectrum IR. The measurements were performed with a resolution of 4 cm^{-1}, 16 accumulations per measurement, in a wavenumber range of 4000–600 cm^{-1}. All samples were then analysed by Gas Chromatography-Mass Spectrometry (GC-MS). Lipids were solvent extracted and analysed following previously published methods (Regert et al., 2006) and a modified version of the protocol presented in Birkemeyer et al. (2016) for samples extracted with cotton swabs. The analyses were performed on an Agilent 7890B GC with a split/splitless inlet, coupled with an Agilent 5977B EI MSD, an FID, and a splitter with corresponding EPC pressure control. The GC was fitted with a nonpolar Agilent J&W DB5 MS column (30 m × 0.25 mm i.d.; 0.25 µm film thickness). The chromatograms and resulting mass spectra were interpreted using the National Institute of Standards and Technology (NIST) library (Version 2.2).

Results

Post-Depositional Traces and Modern Contamination

Old and modern alterations are visible on all tools. The former consists of patination and surface modifications (Fig. 2a) due to taphonomic processes and the depositional environment. Modern day contamination mostly derives from handling, storing, and curating the material and consists of modern fractures and edge-damage (Fig. 2b, c), ink and varnish from labelling (Fig. 2d, e, f), modern glue staining (Fig. 2g), and pencil and pen marks (Fig. 2h, i). On almost all tools, and especially the retouched ones, we observed evidence of pencil. On formal tools, the pencil was used to draw the retouch negatives, hindering the observation of potential wear traces and contaminating the residue.

Modern day pencil lead is a mixture of graphite, clay, and additives like fats (David et al., 2017) and this must be considered when interpreting the results of residue analysis. Similarly, transparent varnish, used to coat the labelling on the tools, hindered the observation of use-wear and residues on some tools, especially small ones such as bladelets and tool fragments. Most varnishes are a mixture of resins, oils, drying agents, and volatile solvents. Resins can be natural as well as synthetic. Ink is a complex mixture of, among other materials, resins, alcohol, solvent, carbon, and pigments. When analysed with the SEM-EDX, all areas covered in clear varnish and ink display strong C concentration (Fig. 3a, b). Additionally, all tools display, in varying proportions, dark, small, angular residues scattered across their surfaces, as visible in the backscattered electron images (see Aleo et al., 2025). These residues are significantly less abundant on tools that were not labelled (Fig. 3d). The particles likely represent old and modern contamination from storing multiple tools together, sediment particles, or handling-related contaminants such as

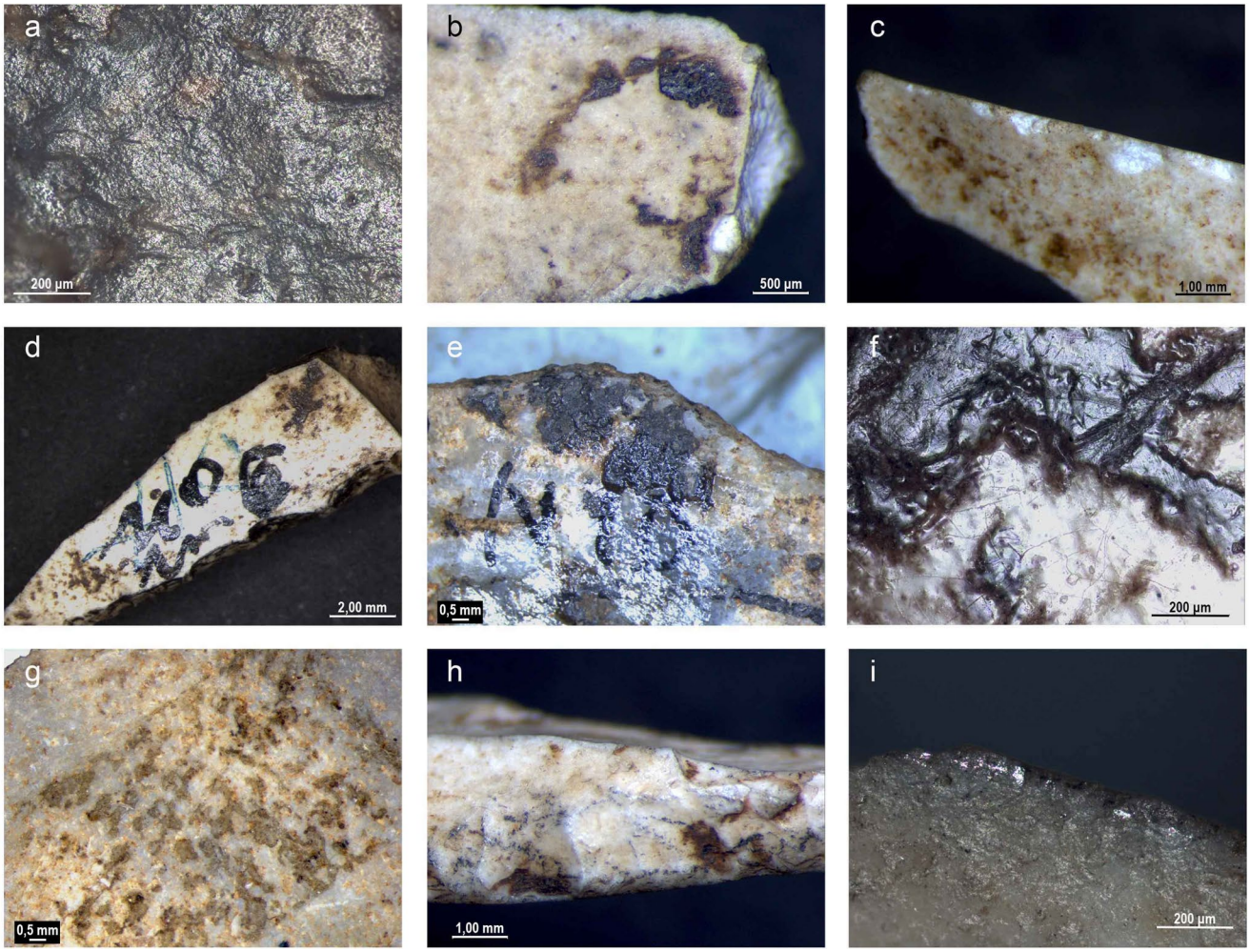


Fig. 2 Selection of post-depositional and modern contamination on Morín tools. (**a**) surface alteration (100x); (**b**) modern tip fracture (25x); (**c**) modern edge-damage (12.5x); (**d**) ink, pencil, and clear varnish from labelling (7.5x); (**e**) clear varnish partially covering a residue (7.5x); (f) close-up of the varnish partially covering a residue (100x); (g) modern glue stain (7.5x); **h-i**) pencil marks (12.5x, 100x)

skin flakes (Frahm et al., 2022; Pedergnana et al., 2016; Taipale et al., 2022b). For labelled tools, some of these particles likely represent varnish fragments that have deteriorated over time and been re-deposited on other areas of the tools.

Residue Analyses (Optical Microscopy, SEM-EDX, Micro-Raman, ATR-FTIR, GC-MS)

Twenty-one tools display a black/brownish residue, which is usually smooth and matte, but occasionally granular (Fig. 4a, b). When thin, the residue is flat with angular terminations. Sometimes thin, flat, brownish, semi-translucent/translucent residues are associated with this group (Fig. 4c). Seven tools display a brown to orange residue, smooth and matte, and with a rounded shape (Fig. 4d). When the residue is very thin, it is flat and angular. Cracks are sometimes present on the surface. Sporadically, dark angular inclusions and possible ochre grains are visible in this residue (Fig. 4e). Two tools display a combination of the previously mentioned residue types. One tool displays a reddish granular residue with clear limits and angular terminations.

Eleven tools with microscopic residues (<1 mm) were analysed with SEM-EDX (SI, Tables S2-S12). For three out of 11 tools (MOR2, MOR9, and MOR13), carbon (C) is the most abundant element; furthermore, sulphur (S) was consistently registered (Table 3). Sulphur, together with calcium (Ca) and potassium (K), is linked in the literature with birch tar (Dinnis et al., 2009; Pawlik & Thissen, 2011); however, more recently this interpretation was challenged, and Ca, K, and/or S were related to the weathering of organic materials (Despotopoulou, 2022). However, in addition to C, S, K, and Ca, these residues display also low sodium (Na) and chlorine (Cl) which are characteristics of skin flakes and may indicate contamination during handling (Pedergnana et al., 2016). The presence of dark-coloured particles on the

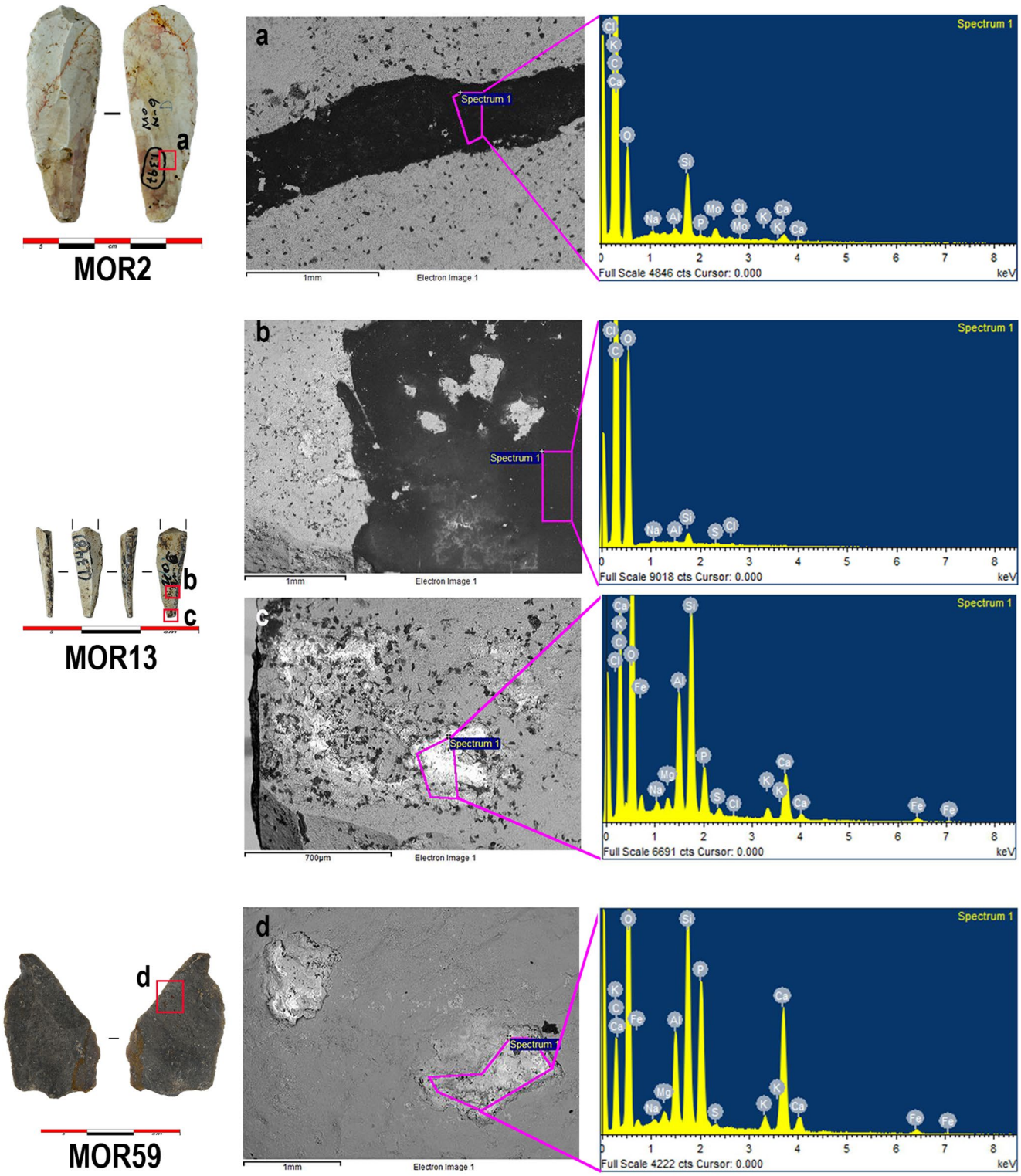


Fig. 3 Surface comparison between labelled (MOR2 and MOR13) and unlabelled (MOR59) tools and EDX-determined elemental composition of the labelling ink and residues

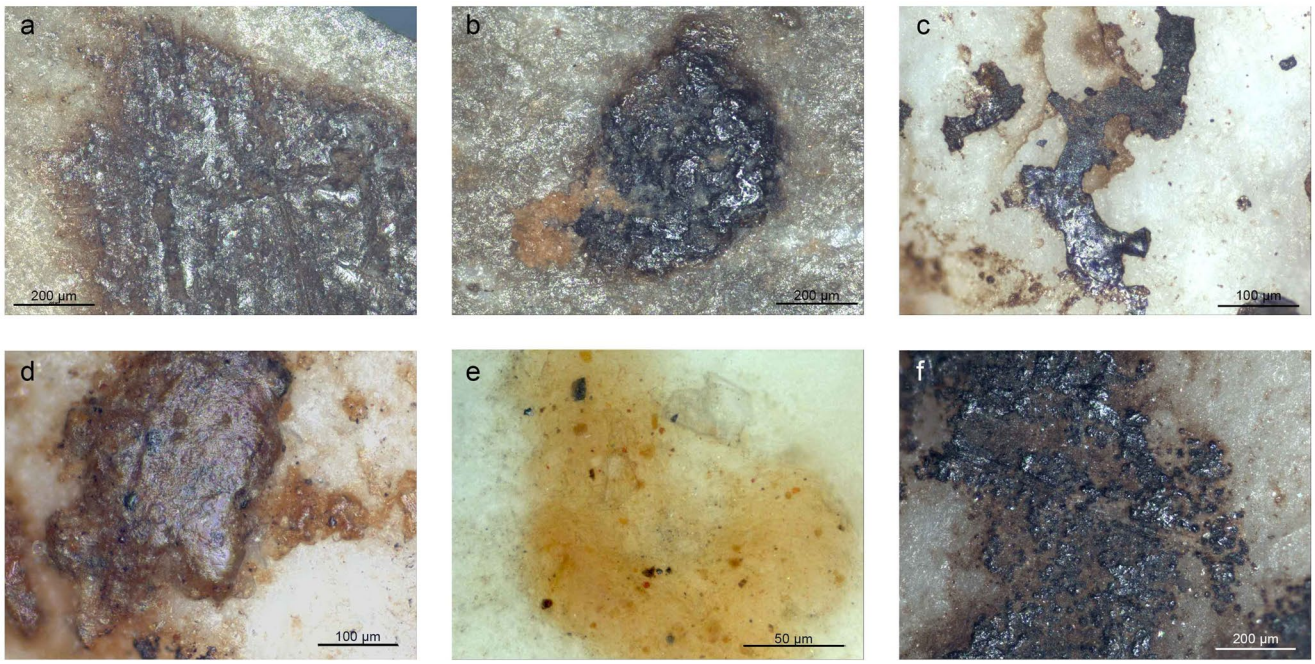


Fig. 4 Selection of residues on Morín tools. a-b) black/brownish residues on MOR5 (**a**) and MOR6 (**b**) (100x); **c**) flat, brownish, angular residue with some cracks on the surface on MOR49 (200x); **d**) orange, smooth, and rounded residue with dark inclusions on MOR2 (200x); **e**) close-up on a residue spot with granular reddish inclusions on MOR2 (500x); **f**) manganese staining on MOR46 (100x)

Table 3 Element weight% (wt%) for tools with potential organic residues. *The average of values measured in the different residue spots is reported. The Dash symbol (-) means that the element was not identified

Element	MOR2			MOR9			MOR13		
	Residue* Wt%	Ink Wt%	Rock Wt%	Residue* Wt%	Ink Wt%	Rock Wt%	Residue* Wt%	Ink Wt%	Rock Wt%
Carbon (C)	28.0	82.5	11.9	40.8	81.9	11.4	34.7	58.6	10.4
Oxygen (O)	53.1	14.5	53.0	41.2	15.7	53.4	49.8	40.5	60.0
Sodium (Na)	0.4	0.1	-	0.3	0.2	-	0.3	0.12	0.3
Magnesium (Mg)	0.4	-	-	0.3	-	-	0.3	-	0.2
Aluminium (Al)	3.9	0.1	-	2.67	0.1	-	2.8	0.1	2.4
Silicon (Si)	6.6	1.4	35.1	4.7	0.8	35.2	5.7	0.5	20.1
Phosphorus (P)	2.1	0.1	-	2.8	-	-	1.8	-	1.2
Sulphur (S)/Molybdenum (Mo)	0.9	0.8	-	0.7	0.7	-	0.3	0.11	0.7
Chlorine (Cl)	-	-	-	0.1	-	-	0.1	0.10	-
Potassium (K)	0.6	0.1	-	0.6	0.2	-	0.6	-	0.6
Calcium (Ca)	3.1	0.4	-	4.7	0.5	-	2.8	-	2.1
Titanium (Ti)	0.1	-	-	0.2	-	-	-	-	0.1
Iron (Fe)	0.9	-	-	0.8	-	-	0.8	-	1.8

residue spots further complicates interpretation, as they are likely the result of contamination and may have contributed to the organic signal. Importantly, the detected elements on MOR2, MOR9 and MOR13 are not exclusive to handling or laboratory contaminants; they may also derive from natural components in the sediment deposits, ancient organic materials, modern contamination, or a combination of these factors.

Additionally, for MOR2 and MOR9, iron (Fe) was registered only in the residue spots, corroborating the observation of possible iron-rich particles made during the examination with optical microscopes (Table 3). MOR59 displays a mixed signal. A high concentration of C was registered in the residue spots, together with S. However, relatively high concentrations of Ca and P were detected in the residue areas. The organic signal may be due to the darked-coloured contaminant visible on the residue deposit while the underlying residue is likely a calcium phosphate deposit formed in the burial environment (Taipale et al., 2022b). MOR4 displays dark and small residues evenly distributed on the surface. Their morphology, distribution and elemental signature suggest that they are modern contaminants, likely

fragments of the clear varnish used for labelling the tool or skin flakes. Six residue samples are inorganic and present a low concentration of C. These inorganic residues present different elemental compositions. Three samples (MOR22, MOR35, and MOR50) are likely manganese oxide (Mn) deposits due to the relatively high proportion of Mn compared to other elements such as aluminium (Al), phosphorus (P), K, Ca, magnesium (Mg), and Fe. MOR50 differs from MOR22 and MOR35 with a higher concentration of Al over Mn. The sample from MOR12 is likely adhering compacted sediment since it presents a more or less equal distribution of Na, Mg, P, S, K and slightly higher proportions of Al, Ca, and Fe. The sample from MOR17 is likely an iron oxide deposit since it presents a high proportion of Fe and significantly lower concentrations of Al, P, zinc (Zn), and Ca. Lastly, the sample from MOR42 is likely a Ca and P deposit since it presents high proportions of Ca and P and a significantly lower concentration of Al. In addition to these elements, all the residue spots analysed display variable concentrations of silicon (Si) and oxygen (O) due to the contribution of the flint substrate.

To better understand the nature of the residue deposits on MOR2, MOR4, MOR9, MOR13, and MOR59, and to evaluate whether they represent modern contamination, ancient organic material, or a combination of both, we conducted micro-Raman spectroscopy. A tool identified as bearing mineral residues thorough SEM-EDX (MOR22) was also analysed as a control sample against those of potential organic origin. The analysis, however, proved inconclusive, as none of the archaeological samples could be reliably confirmed to contain organic residues. Most reference and archaeological samples exhibit Raman spectra that feature a broad band across the complete spectral range, which we attribute to both photoluminescence (mainly 532 nm) and stray light scattering (mainly 785 nm). The Raman peaks in most of the samples appear hidden by this broad band. Only the reference samples of beeswax (532 nm) and pine resin (785 nm) show a rich structure of Raman peaks corresponding to organic compounds due to low level of photoluminescence (Table 4; SI Fig S2, S3, S4). Those peaks closely match pine resin, rosin, and beeswax peaks in the available literature (Bickford & Basu, 2023; Brody et al., 2002; Daher et al., 2010). Inorganic compounds, such as iron oxides and silica derivates, were detected in both the reference and archaeological samples, mostly using the 785 nm laser line (Table 4). Ultimately, Raman spectroscopy did not resolve the identification of residues on MOR2, MOR9, MOR13, leaving their nature uncertain.

Twenty-three residue samples were extracted for GC-MS analysis. Among them, seven samples were selected for ATR-FTIR analysis. ATR spectra of manganese oxide-stained tools (MOR38, MOR44, and MOR46) match well with the spectrum of the cave sediment. The spectra of the remaining tools (MOR11, MOR40, MOR43, and MOR47) present a limited number of low intensity peaks which are absent in the spectrum of the sediment sample (Fig. 5; SI, Table S13). The tools display a doublet of peaks in the region 3000–2800 cm^{-1} (C-H stretching vibrations), of which those in MOR11 have the highest intensity, and a bending vibration band at 1456 cm^{-1}. These bands are characteristics of alkyl fragments (Covi-Schwarz et al., 2017; Vahur et al., 2011). Peaks between 1650–1550 cm^{-1} can be

Table 4 Summary of micro-Raman results for tools with potential adhesive remains and reference samples

Sample	Raman peaks		Interpretation	Reference
	Laser 532 nm	Laser 785 nm		
Pine tar	1531 cm^{-1}	No peaks		
Birch tar	No peaks	No peaks		
Pine resin	No peaks	1646, 1603, 1443, 749, 702 cm^{-1}	Pine resin, Rosin, Colophony	(Brody et al., 2002; Daher et al., 2010; Edwards et al., 1996)
Beeswax	2885, 2728, 1470, 1442, 1302, 1130 1063 cm^{-1}	1652, 1606, 1439 cm^{-1}	Beeswax	(Bickford & Basu, 2023; Edwards et al., 1996)
Pine resin + beeswax	No peaks	1646, 1433, 406, 291, 223 cm^{-1}	Pine resin, Rosin, Colophony, Hematite	(Brody et al., 2002; Daher et al., 2010; Edwards et al., 1996; Hanesch, 2009; Wesełucha-Birczyńska et al., 2012)
Pine resin + beeswax + hematite	No peaks	406, 291, 223 cm^{-1}	Hematite	(Hanesch, 2009; Wesełucha-Birczyńska et al., 2012)
MOR2	No peaks	499, 461, 208, 124 cm^{-1}	α-Quartz	(Hazen, 1988)
MOR4	556, 482, 416, 337 cm^{-1}	667, 532, 415, 293, 222, 126 cm^{-1}	α-Quartz, Hematite, Maghemite	(Hanesch, 2009; Hazen, 1988; Wesełucha-Birczyńska et al., 2012)
MOR9	No peaks	No peaks		
MOR13	No peaks	No peaks		
MOR22	NA	653, 606, 498, 462, 310, 270, 206, 124 cm^{-1}	α-Quartz, Hematite, Hematite-Goethite-Biogenic Vaterite	(Hanesch, 2009; Hazen, 1988; Wesełucha-Birczyńska et al., 2012)
MOR59	No peaks	No peaks		

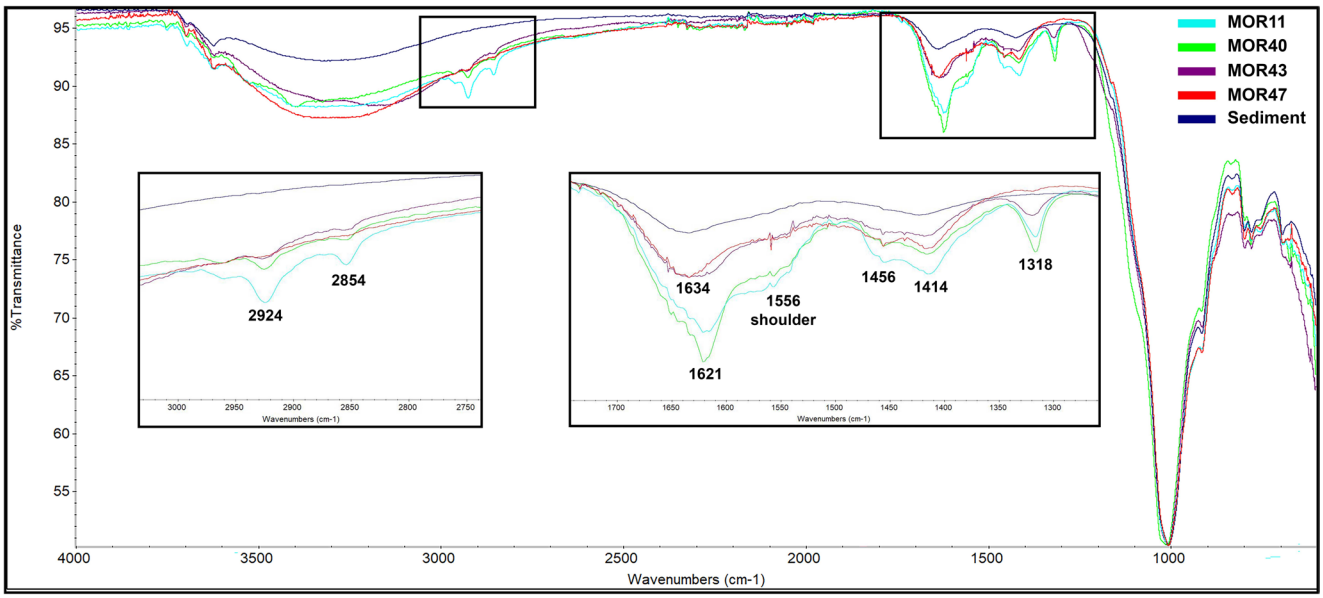


Fig. 5 Comparison of ATR spectra of MOR11, MOR40, MOR43, MOR47, and cave sediment

associated with several functional groups and vibrational modes, including aromatics, proteins/peptides, carboxylates, and alkenes (Pasieczna-Patkowska et al., 2025). Other bands appear at ~1415 cm^{-1} and ~1320 cm^{-1} due to C-H deformations of phenolic groups and carboxylic acids. However, carbonates also present a peak at ~1415 cm^{-1} and the peak at ~1315 cm^{-1} can also indicate cellulose. Some of these bands match with plant extractives such as birch tar and pine resin/tar (Chen et al., 2022; Monnier et al., 2017; Vahur et al., 2011); however, the peaks are not unique to these materials, and they are also present in other plant products, like lignin and cellulose (Monnier et al., 2017; Traoré et al., 2018; Yuen et al., 2009), sediment deposits (Pärnpuu et al., 2022; Tinti et al., 2015), and stratum corneum lipids (Covi-Schwarz et al., 2017).

To rule out handling contamination, we compared the FTIR spectra of MOR11— which displays the most defined peaks— with those of deer skin, keratin from fingernail, and fresh collagen. Reference spectra were obtained from the University of Minnesota Archaeological Materials Infrared Spectra Library and the FTIR library of the Kimmel Centre for Archaeological Science, Weizmann Institute of Science (Fig. 6). In the reference materials, the most intense peaks of keratin and collagen appear in the 1700–1500 cm^{-1} region and correspond to the amide I and amide II bands. The strong peak at ~1650 cm^{-1} represents C=O stretching (amide I, associated with keratin), while the peak at ~1550 cm^{-1} corresponds to C–N stretching of the amino group (amide II). Although the precise wavenumber of the amide I band depends on keratin's secondary structure (Covi-Schwarz et al., 2017), a well-defined amide I–II pattern characteristic of keratinous material is absent in MOR11. Instead, MOR11 shows only weak and poorly resolved features in this region, unlike fresh skin, collagen, or stratum corneum, regardless of secondary structure variability. Notably, in keratin and collagen the amide III protein band dominates the 1300–1200 cm^{-1} region, with a strong peak at 1238 cm^{-1} (Covi-Schwarz et al., 2017; Frahm et al., 2022; Monnier et al., 2017; Olsztyńska-Janus et al., 2018). This diagnostic feature is absent in the archaeological spectrum of MOR11. With respect to alkyl fragments, MOR11 exhibits absorption in the C–H stretching region (3000–2800 cm^{-1}) and in the CH_2 bending band (~1456 cm^{-1}), positions where stratum corneum lipids typically show their strongest signals (Covi-Schwarz et al., 2017). However, this is not unexpected, as many archaeological residues retain degraded lipid or carbohydrate signatures. Such features are not exclusive to stratum corneum lipids or keratin but occur widely in organic substances containing aliphatic chains, including degraded lipids, waxes, and carbohydrates. In skin, these bands are normally much stronger and accompanied by sharp amide I–II–III absorptions and an ester carbonyl band at ~1740 cm^{-1} (Monnier et al., 2018). The absence of these additional diagnostic features in MOR11 indicates that its weak CH bands cannot be uniquely attributed to modern skin contamination.

Among 19 potential adhesive residues analysed by GC-MS, 17 do not contain clear evidence for archaeological adhesives. Only traces of fatty acids and even-numbered long-chain alcohols (C_{18}, C_{28}, and C_{30}) were identified (SI, Table S14). Further, these contain evidence of depositional and post-depositional contamination, such as lipids form phthalates, a fungicide, insecticides, and an insect repellent (SI). However, the remaining two samples, MOR5 and MOR11, have significant preservation of lipid, and unlike

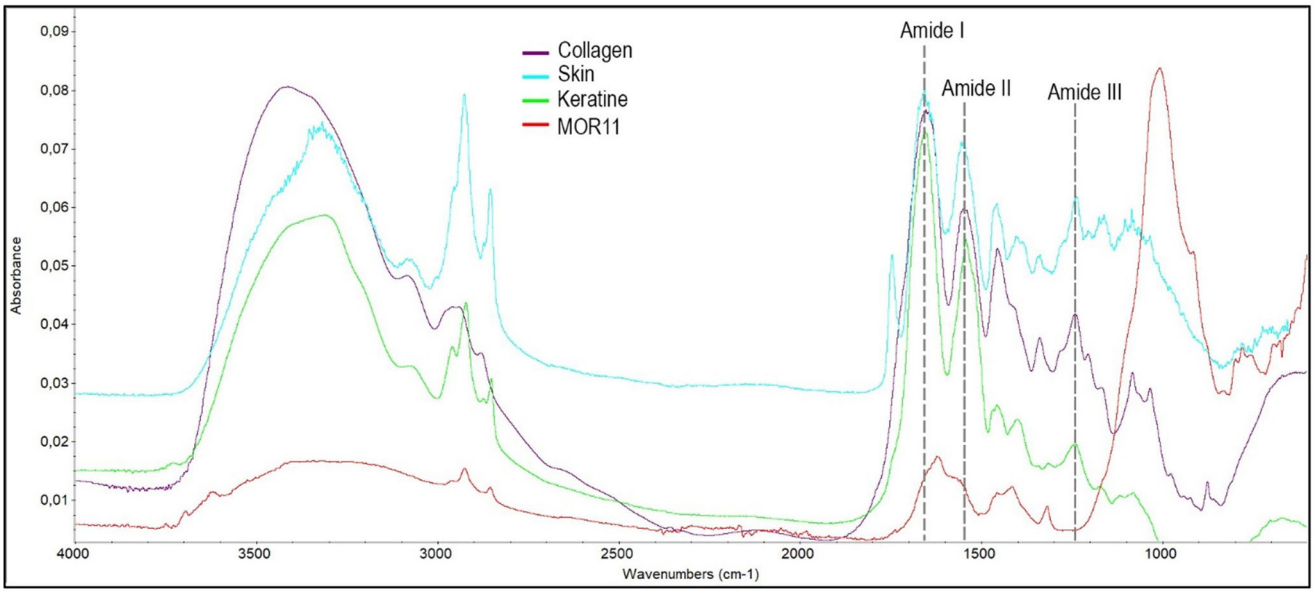


Fig. 6 Comparison between FTIR spectra of collagen (purple), skin (cyan), keratin (green), and MOR11 (red) in the range of 4000–600 cm^{-1}. Comparison spectra are derived from the University of Minnesota Archaeological Materials Infrared Spectra Library and the FTIR library of the Kimmel Centre for Archaeological Science, Weizmann Institute of Science

the other samples, no clear contaminants related to plasticizers, fungicides, and insecticides were identified. Contamination from handling must also be considered. Skin lipids are dominated by cholesterol, squalene, wax esters, triglycerides, and sebaceous fatty acids ($C_{16:0}$, $C_{18:0}$, $C_{18:1}$, branched-chain C_{15}–C_{17}) (Rime et al., 2011). While saturated fatty acids were identified in most samples, including MOR5 and MOR11, these are not unique to skin lipids, and due to the absence of other more diagnostic markers - including those from skin care products (Serb et al., 2024) - contamination from handling is not evident. Therefore, this selective presence of lipids in only two tools indicates that these compounds are not uniformly present across the assemblage and are therefore unlikely to represent common contamination.

The residue sample from MOR5 contains trace amounts of palmitic and stearic acid as well as 1-octacosanol and 1-triacontanol. The bulk of the residue consisted of long-chain *n*-alkanes, ranging from C_{25}-C_{29}, with no clear odd over even preference (Fig. 7a). While this *n*-alkane pattern can be suggestive of sedimentary contamination, this was ruled out because the *n*-alkanes were not identified in a sediment sample collected from layer 5a (S1, Table S14). Instead, the signature may be related to the presence of a wax formed from a plant or insect or a bitumen (Blomquist & Jackson, 1979; Bray & Evans, 1961; Bush & McInerney, 2013; Namdar et al., 2007; Scalan & Smith, 1970), although the absence of wax esters prevalent in plant and animal waxes is concerning. The residue sample from MOR11 contains a high amount of saturated fatty acids, ranging from $C_{8:0}$-$C_{18:0}$ (maximizing at $C_{16:0}$). Two unsaturated fatty acids were also identified: $C_{16:1}$ and $C_{18:1}$. The most unique molecules are lactic acid, totarol, and a totarane ketone (Fig. 7b). Totarol and the totarane ketone are phenolic diterpenoids characteristic of *Cupressaceae* that are native Spain, including *Juniperus thurifera* (Gauquelin et al., 1999). Those molecules were not detected in a sediment sample collected from layer 10 (SI, Table S14); therefore, we can rule out sedimentary contamination. The GC-MS results of MOR11 support the identification of the ATR interpretation of the residue being organic. Conversely, the other three tools (MOR40, MOR43, and MOR47) showing indication of organic compounds in the ATR spectra did not contain any lipids. Therefore, the identified bands may be attributed to sediment contamination and sediment organic matter. It is also possible that the biomarkers concentration was below the detection limit due to the small sample masses used for the analysis (~0.001 gr).

The four residue samples interpreted as manganese stains during optical microscopy investigation were confirmed to not contain relevant organic residues. Two samples (MOR44 and MOR46) do not preserve lipids, while MOR26 and MOR38 display only trace amounts of fatty acids. MOR26 presents $C_{16:0}$ and $C_{18:0}$; the residue sample extracted mechanically from MOR38 presents short- and long-chain saturated fatty acids ($C_{6:0}$, $C_{8:0}$, $C_{9:0}$, and $C_{16:0}$), while the one extracted with the cotton swab imbued with methanol presents only long-chain fatty acids ($C_{16:0}$, $C_{18:0}$). $C_{16:0}$ and $C_{18:0}$ are common compounds found both in plant and animal tissues, but their presence without any other biomarkers suggests contamination, either from the burial environment or post-excavation.

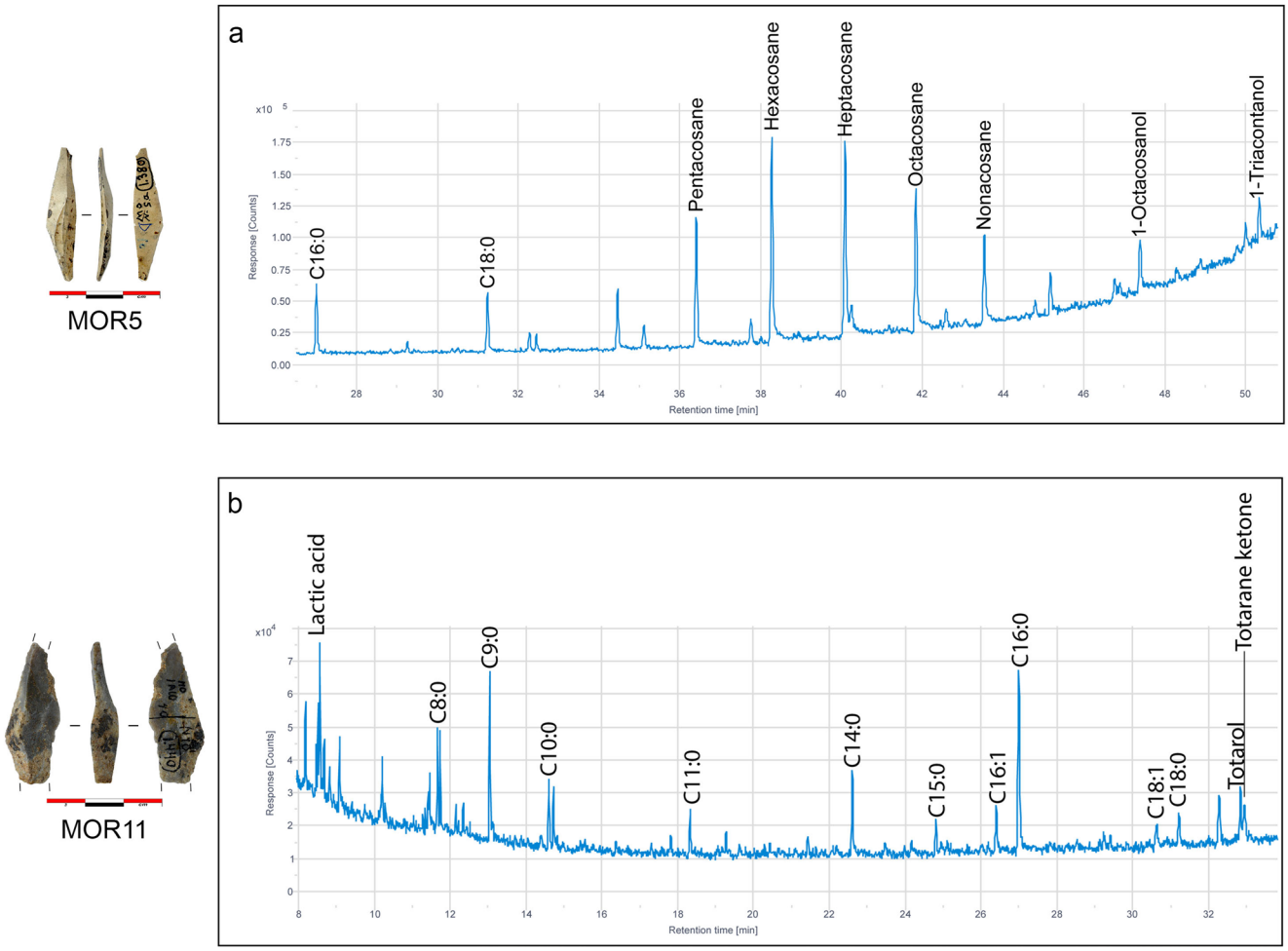


Fig. 7 Partial chromatograms of MOR5 and MOR11 showing the identified molecules

Functional Analysis

Twenty-three of the 35 analysed tools display evidence of use; a detailed description of the observed use-wear traces is provided in the Supplementary Information (SI, Table S1). The worked materials include hide, soft animal tissues, soft to medium-hard plants, siliceous plants, and fresh bone, processed with both transverse and longitudinal motions. In the main text, we focus on tools MOR2, MOR5, MOR9, MOR11, and MOR13, as these specimens yielded residues that may represent ancient organic materials or a mixture or ancient material and moder contaminations. A detailed examination of the distribution of these residues and their associated use-wear traces is therefore critical for interpreting their potential archaeological significance.

MOR2 is a typical Protoaurignacian endscraper on a retouched blade (cf. Aleo et al., 2021) with clear macro- and micro-traces related to hide processing (Fig. 8a, b). Micro residues are mostly distributed in isolated spots on the dorsal and ventral faces (Fig. 9a), excluding the distal portion of the tool. Some residues are associated with lateral edge-removals (Fig. 9b).

MOR5, MOR9, MOR11, and MOR13 show different macro-fracture patterns (for terminology see Coppe & Rots, 2017). MOR5 was described by Bradtmöller et al. (2016) as a discarded preform likely used as a lateral implement based on the distribution of the residue. The proximal extremity exhibits a modern fracture. The distal extremity displays a bending-initiating fracture with a spin-off fracture with a long propagation phase and a hinged termination initiated from the fracture surface and terminated on the right edge (Fig. 8c). Some close and isolated edge-removals, a few with perpendicular orientation, are present on the left edge, especially on the distal area (Fig. 8d). The residue is mostly preserved on the retouch scars of the left backed edge (Fig. 9d). However, residue spots are also visible in other locations of the dorsal and ventral face, covering approximately one-third of the tool (Fig. 9c).

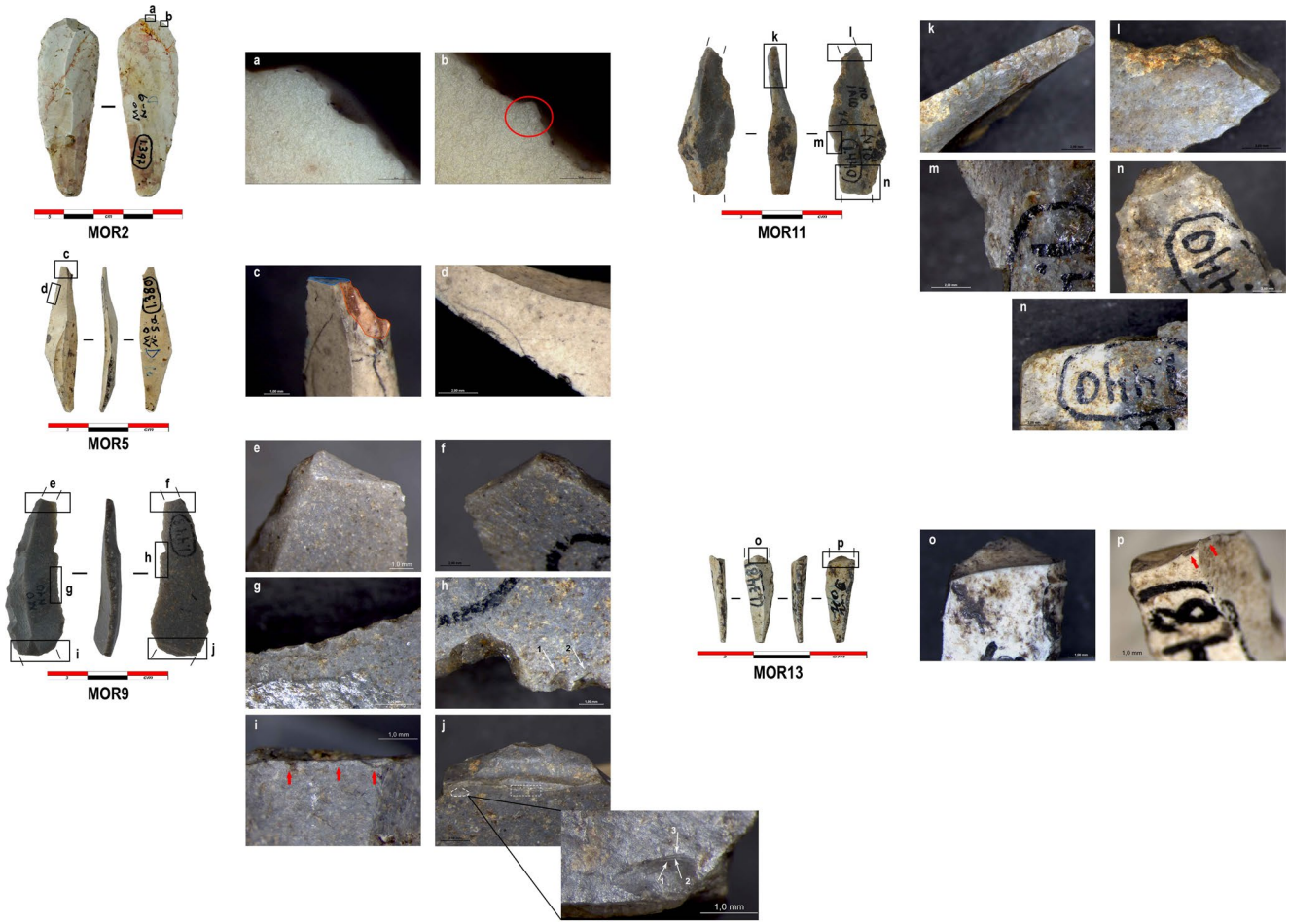


Fig. 8 Use-wear traces on MOR2, MOR5, MOR9, MOR11, and MOR13 interpreted as bearing potential adhesive residues. MOR2: (**a**) edge rounding and greasy polish along the edge; **(b)** intense resharpening of the working edge with minimal use traces visible (red circle) between resharpening scars; MOR5: (**c**) bending-initiating fracture (blue) with a spin-off fracture with a long propagation phase and a hinged termination (orange); (**d**) edge-removals on the distal area; MOR9: **e**-**f**) distal bending fracture; **g**) edge-removals on the dorsal lateral edge with a perpendicular orientation; **h**) edge-removal on the ventral lateral edge with oblique orientation (1) and fissured termination (2); **i**) spin-off scars on the dorsal face; **j**) proximal hinge-to-step terminating fracture and close up of the spin-off scar on the ventral face showing a complex termination; MOR11: **k**) retouched backed edge; **l**) distal snap fracture; **m**) edge-removal with perpendicular orientation of the ventral lateral edge; **n**) proximal bending fracture combined with a burin-like spin-off scar with a long propagation phase and step termination; MOR13: **o**) distal bending fracture with hinged termination; **p**) small spin-off scars initiated from the fracture surface

MOR9 is a backed point that can be typologically described as a typical Châtelperronian point. The point is manufactured on a regular laminar blank, with a slightly curved profile, and displays a continuous retouched back. The tool presents a combination of distal bending fracture initiated from the ventral face (Fig. 8e, f) and a proximal hinge-to-step terminating fracture initiated from the dorsal face (Fig. 8j) with spin-off scars initiated from the fracture surface and terminated on the dorsal and ventral surfaces (Fig. 8i, j). We observed close edge-removals, mostly perpendicular orientation, on the right edge (Fig. 8g). However, some of these lateral scars display an oblique orientation and fissured terminations (Fig. 8h). Isolated and patches of micro residues are observed on the proximal-mesial portion of the back, dorsal, and ventral faces (Fig. 9e, f).

MOR11 is a partially backed point that can be typologically describes as an atypical Châtelperronian point since displays only a partially retouched back. Partially backed Châtelperronian points are not rare in archaeological assemblages ascribed to this techno-complex, and they are documented at Morín (Maíllo-Fernández, 2005) as well as at Grotte de la Verpillière I (Würschem et al., 2024), Grotte des Fées (Würschem et al., 2024), Quinçay (Roussel et al., 2016), among other sites. MOR11 displays a distal snap fracture with an oblique profile (Fig. 8l) and a proximal bending fracture combined with a burin-like spin-off scar with a long propagation phase initiated from the fracture surface and terminated on the right edge (Fig. 8n). The burin-like fracture has a step termination and cuts the edge-removals on the lateral edge. The edge-removals are

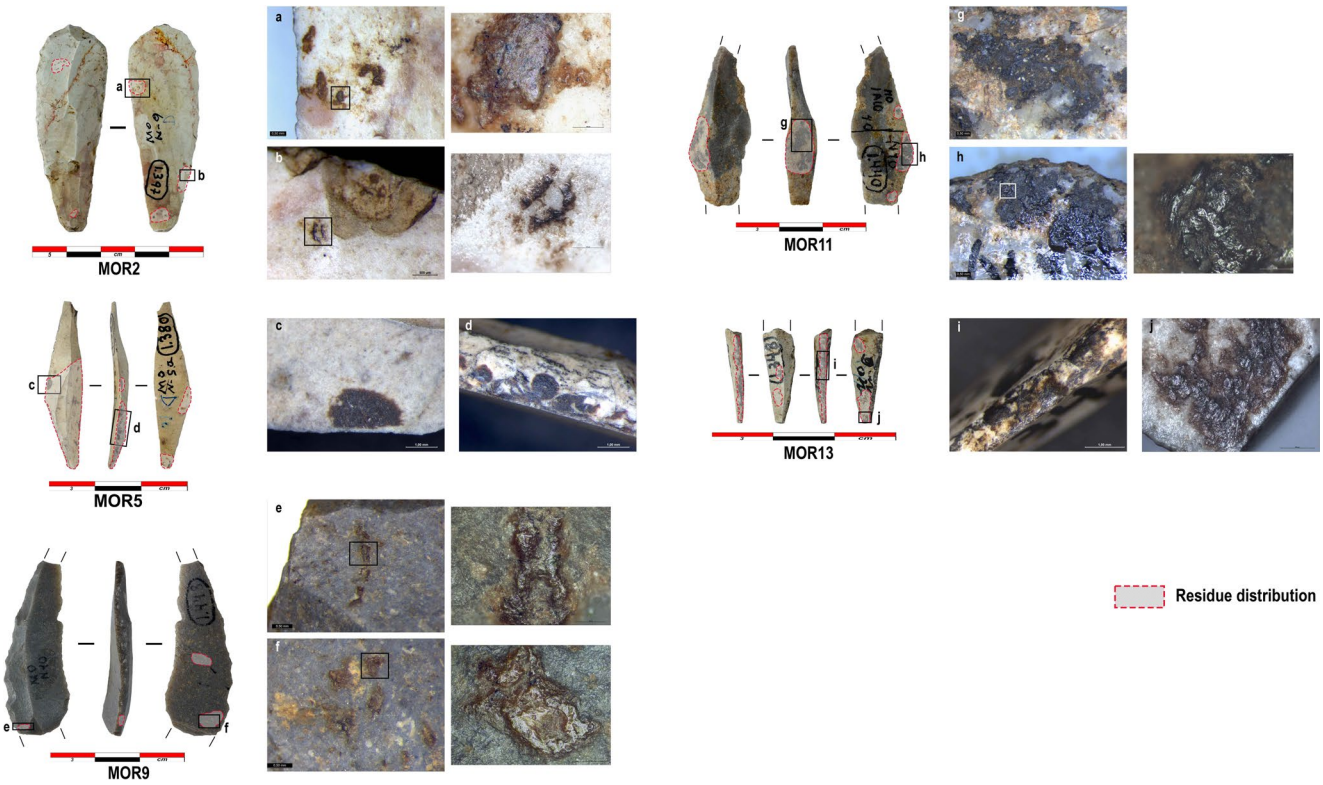


Fig. 9 Distribution and appearance of residues interpreted as potential adhesive remains on MOR2, MOR5, MOR9, MOR11, and MOR13

located on the ventral right edge of the tool; they are regular and close to each other, sometimes overlapping, and with a perpendicular orientation (Fig. 8m). A thick black deposit is found on the mesial left edge of the tool, on the back, dorsal, and ventral surfaces (Fig. 9g, h). The distribution of the residue, limited to the lateral backed edge, closely parallels adhesive residues reported for backed tools in the literature (Lombard, 2008; Sano et al., 2019; Tomasso et al., 2021). However, the presence of a rough inclusion in the stone in this area may account for the preferential preservation of the residue on this side compared to other parts of the tool.

MOR13 is a proximal-mesial fragment of a retouched bladelet displaying bilateral alternate retouch (Dufour bladelet). The left edge presents an inverse, semi-abrupt, continuous retouch. The right edge has a direct, abrupt, continuous retouch. The bladelet displays a distal hinged-terminating bending fracture initiated from the ventral face with small spin-off scars initiated from the fracture surface and terminated on the dorsal surface (Fig. 8o, p). A continuous residue deposit is visible on the lateral retouched edges of the bladelet (Fig. 9i), while patches of residue are distributed on the ventral and dorsal surfaces (Fig. 9j). The traces and the distribution of the residue may suggest the tool was hafted as a straight point.

Based on tools' typology, morphology and the fracture patterns, MOR5, MOR9, MOR11, and MOR13 may have been used as projectiles (Table 5). Weapon elements can be identified if they display specific combinations of macro- and micro-wear evidence (Coppe & Rots, 2017; Metz et al., 2023; Rots, 2016; Rots & Plisson, 2014). The presence of spin-off fractures initiated from an existing bending fracture is considered strong evidence of projectile use, especially when display fissured terminations indicative of strong compression (Coppe & Rots, 2017; Metz et al., 2023; Tomasso et al., 2021). The characteristics of spin-off fractures on MOR5 and MOR13, being small, with a short propagation, and occurring on the surface of break terminations do not allow us to rule-out a non-projectile origin. Conversely, those on MOR9 and the burin-like fracture on MOR11 provide more convincing evidence for their use. Unfortunately, no microscopic linear impact traces (MLITs) could be observed on the studied tools to strengthen our functional interpretation due to the strong post-depositional surface alteration. Additionally, the lateral removals could also not be used as evidence for projectile use as they were preferentially perpendicularly oriented to the axis of the tools and therefore could be related to many processes unrelated to projectile use (Coppe & Rots, 2025; Fischer et al., 1984; Taipale et al., 2022a). The edge-removals in the non-active part of the tools may relate to hafting wear.

However, the absence of associated striations, bright spots, and polish – a typical combination diagnostic of hafting (Rots, 2010; Taipale & Rots, 2020) – makes the identification of hafting traces ambiguous.

Discussions

We conducted a detailed examination of 31 stone tools and their residues from Morín Cave to assess evidence for adhesive use at the site. However, the overall poor preservation of residues, the likelihood of post-depositional contamination, and the inconsistent application of analytical techniques due to sampling constraints mean that only cautious interpretations are possible.

Among the analysed tools, five specimens (MOR2, MOR5, MOR9, MOR11, and MOR13) were identified as potential candidates for ancient adhesive residues based on the residues' surface characteristics, spatial distribution, and molecular signatures. In this section, the results of our multi-analytical protocol will be critically evaluated to test this interpretation and to determine whether adhesive technology can be reliably inferred at Morín Cave.

Adhesive Technology at Morín Cave: Where do we Stand?

The first step in identifying adhesive residues was based on their morphological characteristics. The residues on MOR2, MOR5, MOR9, MOR11, and MOR13 display features and surface characteristics consistent with other archaeological and experimental adhesive remains previously described (Aleo et al., 2023, 2024; Lombard & Wadley, 2007). However, as noted in earlier studies, optical microscopy alone is unreliable for identifying and differentiating between adhesive materials (e.g., Aleo et al., 2024; Soriano et al., 2015). Furthermore, residues that appear to be tar or resin may, upon biomolecular analysis, correspond to environmental, mineral, or burial-derived substances (Croft et al., 2018; Taipale et al., 2022b).

SEM-EDX analysis of residue deposits on MOR2, MOR9, and MOR13 yielded a complex picture due to likely sources of modern contamination. Back-scattered electron images of all three tools show dark-coloured particles overlapping the lighter-coloured residues. Despite attempts to measure residue spots with minimal contamination (for measured locations see Aleo et al., 2025), these dark-coloured particles likely contributed to the recorded SEM-EDX signal. Consequently, the results should be interpreted cautiously, as the data likely reflect a mixed signal. Without further evidence from the micro-Raman analysis supporting their interpretation as adhesives, the most likely interpretation is that the black contaminant particles contribute to most of the carbon (C) signal, while the residues themselves are likely mineral in origin (Table 6). The elements detected in the residue spots are consistent with skin flakes (Pedergnana et al., 2016) and with the clear varnish and ink used for labelling the tools, both of which exhibit strong carbon signals and thus represent probable sources of the measured C.

Overall, the residue deposits are most likely mineral in origin, possibly resulting from natural iron oxide deposition or the formation of silicate, carbonate, or sulphate crusts in the burial environment. This interpretation is supported by their light colour in back-scattered images, elemental composition, and visual comparison with similar archaeological mineral residues (Croft et al., 2018; Rots et al., 2024; Taipale et al., 2022b).

Table 5 Summary of use-wear results of artefacts with possible adhesive residues analysed in this study. Artifacts indicated with *were also analysed by Bradtmöller et al. (2016). Degree of confidence related to the interpretation of use-wear traces: + low certainty, ++ moderate certainty; +++ high certainty; ++++ certain

ID	Cultural affiliation	Tool type	Use-wear	Interpretation	Functional interpretation degree of confidence
MOR9	Châtelperronian	Backed blade (Châtelperronian point)	Combination of proximal bending break + spin-off scars on dorsal and ventral face	Projectile	++
MOR11	Châtelperronian	Partially backed blade	Combination bending break + spin-off burin-like fracture with long propagation and step termination	Projectile	++
MOR2	Protoaurignacian	Endscraper	Edge-rounding + micro-polish	Scraping hide	+++
MOR13	Early Aurignacian	Dufour bladelet	Combination of bending break + small spin-off scars on dorsal face	Projectile	+
MOR5/ Artifact C*	Gravettian	Partially backed blade	Combination of bending break + spin-off scar on lateral edge	Projectile	+

Table 6 Summary of residue analysis results for artefacts with possible adhesive residues analysed in this study. Artifacts indicated with * were analysed by Bradtmöller et al. (2016). Degree of confidence related to the interpretation of residues: + low certainty, ++ moderate certainty; +++ high certainty; ++++ certain

ID	Cultural affiliation	Tool type	Residue interpretation	Additives	Method of analysis	Residue interpretation degree of confidence
MOR9	Châtelperronian	Backed blade (Châtelperronian point)	Mineral deposit + organic contaminants	No	SEM-EDX	++/+++
MOR11	Châtelperronian	Partially backed blade	Adhesive: Juniper resin or tar	No	FTIR, GC-MS	++
MOR2	Protoaurignacian	Endscraper	Mineral deposit + organic contaminants	No	SEM-EDX	++/+++
MOR13	Early Aurignacian	Dufour bladelet	Mineral deposit + organic contaminants	No	SEM-EDX	++/+++
MOR5/Artifact C*	Gravettian	Partially backed blade	Adhesive: possibly degraded plant or insect wax or weathered bituminous material	No	SEM-EDX*, micro-Raman*, GC-MS	++
Artifact B*/MOR1	Protoaurignacian	Partially backed blade	Adhesive: proteinaceous or resinous material	Burnt bone?	SEM-EDX*, micro-Raman*, FTIR*, GC-MS	+/++
Artifact A*	Gravettian	Backed blade	Adhesive: proteinaceous or resinous material	Ochre?	SEM-EDX, micro-Raman, FTIR	+/++
Artifact D*	Gravettian	Burin	Adhesive: resinous material	No	SEM-EDX, micro-Raman	+

The chemical signature of MOR11 residue allows for a more confident interpretation of its nature. The infrared spectrum of MOR11 shows a mixture of organic compounds and inorganic phases matching those observed by Bradtmöller and colleagues in a previous study and interpreted as possibly indicating fatty materials or resins (Bradtmöller et al., 2016). Our comparative analysis of spectral peaks and overall band shapes ruled out the possibility that the residue derives from modern handling contamination. This was further corroborated by GC-MS results.

The molecular of MOR11 indicates the residue originates from an exudate (resin or tar) from a tree of the *Cupressaceae* family, such as *Juniperus thurifera* due to the presence of characteristics phenolic diterpenoids (Table 6). Palynological data from Morín (Leroi-Gourhan, 1971) should be taken with caution considering the inconsistency of the pollen record. Yet, other studies from this area indicate that the transition between the end of the Mousterian to the Aurignacian was characterised by a shift to more arid and cooler climatic conditions accompanied by a reduction of forest masses. In this cold and dry environment, conifers were the most represented taxa, with *Pinus* being the most abundant species, followed by *Juniperus*, *Fabaceae*, and *Salix* (Allué et al., 2018; Fernández-García et al., 2023; Ochando et al., 2022). Therefore, Pine and Juniper species were locally available in the environment surrounding the cave. Furthermore, *Pinus* and *Juniperus* charcoals are commonly recovered in Late Mousterian and Aurignacian sites of the Iberian Peninsula (e.g., Badal et al., 2011), attesting the wider exploitation of this taxa.

Considering the available data, MOR11 was likely used as a projectile point, as suggested by the use-wear, which in turn implies that it was hafted. Supporting this interpretation, the residue is spatially restricted to the backed edge of the tool, a distribution closely matching adhesive residues reported for backed tools in the literature. Furthermore, chemical analysis revealed a high concentration of lipids, including compounds characteristic of conifer plants, which were not detected in any of the sediment control samples or in the other tools analysed. While we acknowledge that the current data cannot provide absolute certainty, the convergence of functional, spatial, and chemical evidence makes it plausible that the residue represents the remains of an adhesive used in hafting.

Regarding MOR5, SEM-EDX and Raman data are reported in Bradtmöller et al. (2016). Based on the available figures, the residue appears as a dark, compact, and homogeneous deposit, with no dark-coloured, angular particles suggestive of contaminants. The residue shows a strong C contribution, the presence of S, and low-intensity signals of Al, K, and Fe. In addition, a high-intensity Ca region overlain by P is observed. However, the study does not provide a complete list of all detected elements in the deposit nor their weight percentages. The Raman results are dominated by intense fluorescence, which obscures the bands of organic materials. Nevertheless, bands at ~1300 cm^{-1} and ~1600 cm^{-1}, related to C–C bonds and assigned to charcoal in different states of crystallization, are reported. The publication presents only a partial Raman spectrum limited to these peaks, preventing a broader evaluation. For these reasons, and as already noted

by Bradtmöller et al. (2016, p. 11), the interpretation of the residue as glue remains uncertain.

The GC-MS signature of the sample from MOR5 presented in our analysis, consisting of long-chain *n*-alkanes (from C_{25}-C_{29}) with no clear odd over even preference, could be attributed to a variety of sources (Table 6). A degraded plant or animal wax should be considered first, as such waxes can lose their more labile molecular markers over time due to taphonomic processes. Specifically, the signature is similar to degraded dark beeswax (Namdar et al., 2007). However, no other biomarkers of beeswax were identified in the sample, so this must be considered a cautious interpretation. Beeswax is used as an additive in hafting adhesives as a plasticizer (Kozowyk et al., 2016) or used in its pure form as an adhesive on its own. Beeswax has been mixed with conifer resin in the Neanderthal site of Fosellone Cave (Degano et al., 2019), while pure beeswax was used hafting material for a Late Upper Palaeolithic barbed bone point at Bergkame (Baales et al., 2017). Evidence of exploitation of bee products and beeswax in Iberia dates to later periods; beeswax and propolis were identified inside ceramic vessels as funerary offers or sealants in Bronze Age and Iron Age contexts (Frade et al., 2014; Parras et al., 2015).

The GC-MS results of MOR5 could also be interpreted as related to the use of bitumen, which contains a similar *n*-alkane profile (Scalan & Smith, 1970). The absence of steranes, terpanes and hopanes, typical bitumen markers (Nardella et al., 2021), is compatible with either strong degradation, low-abundance residues, or the limitations of solvent-based GC–MS. Bitumen is a well-known hafting material, and evidence for bitumen adhesives is present in Europe (Doronicheva et al., 2022) and the Levant (Boëda et al., 2008b). In Iberia, molecular analysis supports the use of bitumen, with it identified in the dental calculus of a Neanderthal individual in the northern Iberian site of El Sidrón (Hardy et al., 2012). This was connected to non-dietary activities such as using the mouth as a third hand, likely during the process of hafting stone tools with bitumen adhesives. The same individual also presented activity-related dental wear, particularly chipped enamel, supporting this hypothesis (Hardy et al., 2012; Radini et al., 2016, 2017). Several bitumen sources are available in Spain, including one at Lames de Parres in Asturias, located 15 km from El Sidrón and at Punta del Cuerno in the modern coastline of Cantabria, located ~30 km from Morín Cave (Kruge & Suárez-Ruiz, 1991). The latter would have been the likely source of bitumen for hunter-gatherers groups inhabiting Morín.

For MOR5, the use-wear data are inconclusive, and its function cannot be firmly established. Nevertheless, the residue distribution suggests that it may have been hafted as a lateral implement on an organic shaft (see Bradtmöller et al., 2016). Although the chemical signature is incomplete, the combination of residue distribution and chemical data suggests that MOR5 was plausibly hafted, even if the exact adhesive cannot be definitively identified.

In addition to the tools analysed here, adhesive residues have previously been reported at Morín on two Gravettian (artefacts A, D) and one Aurignacian (artefact B) implements (Bradtmöller et al., 2016). Based on SEM-EDX, micro-Raman, and FTIR, these residues were interpreted as possible natural resin and/or proteinaceous material on artefacts A and B, and as natural resin on artefact D. For artefact A, burnt bone was described as a filler, while for artefact B ochre was noted (Table 6). However, these identifications require critical reassessment in light of our new analyses. In the case of artefact D, the interpretation of resin rests mainly on the detection of sulphur by SEM-EDX and C–H stretching bands (3000–2850 cm^{-1}) in vibrational spectra. This combination is only suggestive of an organic residue and is not sufficient to confirm resin, especially since sulphur signal may originate from many sources. The interpretation of the residues on artefacts A and B relies mostly on the ATR spectra patterns showing an admixture of organic and mineral components. The functional groups present in the spectra likely represent degrade lipids or resinous materials - due to the presence of CH stretches at ~2920/2850 cm^{-1}, the ester C=O at ~1738 cm^{-1}, C-H deformation (alkyl groups) between 1456–1370 cm^{-1} (Monnier et al., 2018; Vahur et al., 2011)- while the clear absence of Amide II and III bands argues against modern skin lipids contamination. Overall, while FTIR features include resin-like bands, these are non-specific, and without molecular biomarkers they cannot support a confident claim of plant resin. GC-MS analysis of artefact B (MOR1 in our analysis) failed to detect diagnostic molecular markers. This negative outcome does not exclude the presence of resin or other organics, but it underscores that the available evidence remains dubious.

Regarding the use of mineral fillers, Bradtmöller et al. (2016) identified burnt bone in artifact A, based on the strong Ca and P signals detected in the EDX spectra and corresponding FTIR bands (Bradtmöller et al., 2016, p. 9). While the detection of calcium phosphate may indeed indicate the presence of osseous material (cf. Monnier et al., 2018), it can also form authigenically in the burial environment as a result of diagenetic processes (Taipale et al., 2022b). Consequently, in the absence of additional analyses and supporting evidence, the interpretation of burnt bone particles intentionally added as loading agents should be treated with cautions.

Artifact B was interpreted as containing an adhesive loaded with ochre based on the presence of a strong Fe signal in the EDX scan, as well as characteristic FTIR and Raman peaks. The authors interpreted this as evidence that ochre had been deliberately added as a loading agent to enhance the adhesive's properties (Bradtmöller et al., 2016). During the screening of the collection, we frequently documented ochre in the form of small iron oxide nodules across the Upper

Palaeolithic layers of Morín, as well as in Mousterian and Châtelperronian contexts (see also Bradtmöller et al., 2016). These nodules showed no macroscopic traces of use, and no detailed microscopic examination was conducted, as this lay beyond the scope of the present analysis. Nevertheless, evidence from other sites indicates that iron oxide nodules were sometimes worked to produce ochre powder in Mousterian, Châtelperronian, and Upper Palaeolithic contexts, demonstrating that both Neanderthals and AMH employed ochre for a range of purposes, including as a loading agent in adhesives. Experimental studies have shown that the addition of ochre modifies the material properties of adhesives, increasing their strength and improving their workability (Kozowyk et al., 2016; Tydgadt & Rots, 2022; Wadley, 2005; Zipkin et al., 2014). However, as Bradtmöller et al. (2016, p. 11) themselves noted, the absence of control Raman and FTIR measurements outside the residue spots, as well as a lack of comparative sediment analysis, prevents a definitive exclusion of the possibility that the ochre derives from the burial environment rather than from anthropogenic addition.

Adhesives Technology at Morín Cave: Materials, Functions, and Limitations

The multi-analytical approach undertaken in this study allow us to discuss some aspects of adhesive technology at Morín Cave and contributes to the broader discussion on the identification of Palaeolithic organic residues.

Possible adhesive residues were observed on MOR5, MOR11, artefact A, and artefact B, based on their chemical signatures, location, and distribution, although none yielded a clear or unambiguous identification. These residues derive from the Châtelperronian (MOR11), Aurignacian (artefact B), and Gravettian (MOR5 and artefact A) layers, making Morín one of the few sites where potential adhesive residues spanning several Upper Palaeolithic technocomplexes have been chemically identified. Our results suggest that different adhesive materials were likely exploited, including conifer resin (MOR11) and plant or animal wax or bitumen (MOR5), while for artifacts A and B a cautions interpretation as proteinaceous material/natural resin was proposed due to the absence of secure molecular data (Bradtmöller et al., 2016). Use-wear traces suggest that MOR11 may have been used as a projectile, whereas for MOR5 the wear evidence does not allow a confident functional interpretation. Artefacts A and B have been interpreted by Bradtmöller et al. (2016) as distally hafted points based on their fracture patterns and comparison with published references.

Unfortunately, the limited number of potential adhesive remains identified prevents us from establishing a chronostratigraphic framework for adhesive technology at the site, or from comparing Neanderthal and AMH adhesive traditions.

Methodological Considerations

Our analysis emphasizes the importance of applying a comprehensive analytical approach to the study of ancient adhesives. This approach systematically integrates traceology with elemental and molecular analyses, enabling researchers to overcome the limitations inherent to individual methods when identifying archaeological residues.

A detailed examination of the objects using both low- and high-power microscopy allows for the interpretation of the tool's context of use and the evaluation of morphological features of residues. This includes their distribution, surface characteristics, and association with wear traces, which aids in distinguishing ancient or use-related residues from modern contamination (Cnuts & Rots, 2017).

Building on these morphological observations, scanning electron microscopy (SEM) coupled with energy-dispersive X-ray (EDX) analysis can help distinguish residues with high organic content from mineral deposits. However, SEM-EDX is primarily limited to verifying the organic nature of residues; its use alone is insufficient to fully identify organic substances (Despotopoulou et al., 2024; Monnier & May, 2019). Many signals detected may derive from a wide range of modern or ancient sources, requiring careful evaluation alongside complementary analytical methods.

Spectroscopic techniques, including Fourier-transform infrared (FTIR) and Raman spectroscopy, provide molecular-level information and are widely applied in the characterisation of archaeological residues (Bordes et al., 2017; Monnier et al., 2017, 2018; Prinsloo et al., 2013). Their diagnostic power is constrained by broad characterisation bands that are rarely material-specific, degradation of organic components, weak or noisy spectra, and the absence of extensive reference libraries (Despotopoulou et al., 2024; Monnier et al., 2017). In situ FTIR reflectance measurements generally produce spectra of lower clarity compared to invasive applications that require residue sampling (Despotopoulou et al., 2024). When possible, attenuated total reflectance (ATR) FTIR is recommended as it can enhance spectral quality by improving the visibility of weak bands and reducing background effects. However, in situ application is not fully non-invasive and carries a risk of damaging fragile archaeological materials.

For Raman spectroscopy, long-wavelength laser excitations (e.g., 1064 nm–785 nm) are recommended for materials that have undergone environmental degradation or exhibit high background fluorescence, such as ancient and modern resins (Daher et al., 2010; Edwards & Ali, 2011). Even with a 785 nm laser, however, some residual fluorescence is expected, as we directly observed in our analysis. Our work might have benefited from the use of a 1064 nm near-infrared laser, given its greater ability to suppress

fluorescence, though higher laser power increases the risk of damaging archaeological samples. Nonetheless, as noted in previous studies, thin, small, and weathered samples often produce noisy spectra with low signal-to-noise ratios that are difficult to interpret (Asquier et al., 2009; Daher et al., 2010).

FTIR and Raman spectroscopy are also valuable for identifying inorganic components, such as mineral fillers (e.g., ochre) in adhesive formulations (Prinsloo et al., 2023; Wojcieszak & Wadley, 2018). The production of compound adhesives reflects sophisticated knowledge of material properties and complex executive functions, including abstraction, forward planning, and multitasking (Wadley, 2010, 2013) and thus plays a key role in understanding the technological complexity associated with adhesive manufacture. In this context, spectroscopy can corroborate observations made by microscopy and SEM-EDX, providing more accurate chemical identification. To distinguish anthropogenic residues from natural mineral deposits, analyses of sediment, control samples outside residue spots, and residue distribution are essential (Prinsloo et al., 2023; Wojcieszak & Wadley, 2018). Complementary techniques, such as X-ray diffraction (XRD) and micro-computed tomography (µ-CT), further strengthen interpretations. XRD provides crystallographic information that can unambiguously identify mineral phases even in mixtures, while µ-CT allows virtual sectioning of residues to evaluate particle distribution (Aleo et al., 2024).

Gas chromatography–mass spectrometry (GC-MS) remains among the most precise methods for characterising unknown organic residues, offering detailed molecular fingerprints (Evershed, 2008; Langejans et al., 2022). Its limitations include its destructive nature and the complexity of chromatogram interpretation. Biomarkers identification relies on reference collections and may be affected by natural degradation, burial conditions, or anthropogenic modifications such as thermal processing (Polla & Springer, 2022; Whelton et al., 2021). Furthermore, many biomarkers are not material-specific and occur in multiple natural sources, meaning their detection alone cannot definitively confirm the use of a particular resource (Polla & Springer, 2022; Whelton et al., 2021). Different extraction protocols preferentially detect certain compound classes: liquid chromatography–MS (LC-MS) is suited for large biomolecules, whereas pyrolysis GC-MS (py-GC-MS) is appropriate for very small samples (<1 mg) (Cleland & Schroeter, 2018; Whelton et al., 2021). For MOR5, py-GC-MS could have been particularly valuable in confirming or excluding bitumen biomarkers, as it targets the heavy, insoluble fraction that solvent-based GC-MS may miss. Therefore, although GC-MS provides the most detailed characterisation of organic residues, its results must be interpreted alongside complementary analytical techniques, as it cannot reliably serve as the sole method for residue identification.

Conclusions

Morín Cave stands out as one of the few sites where Palaeolithic residues have undergone intensive multi-analytical investigation for both identification and characterisation. Our study demonstrates the importance of a multi-step analytical protocol, combining microscopic use-wear analysis with multiple complementary analytical methods, for accurate interpretation of ancient residues and for distinguishing them from post-depositional contamination.

Applying this rigorous methodology to the Morín assemblage, despite its suboptimal preservation, allowed us to identify potential adhesive residues on several tools. Evidence suggests the presence of adhesives on a Châtelperronian point (MOR11) and on a Gravettian tool (MOR5). At Morín, adhesives were likely used to haft tools for projectile purposes. GC-MS analyses indicate that resin or tar from plants in the *Cupressaceae* family was applied to the Châtelperronian point, whereas potential insect wax, plant wax, or bitumen was identified on Gravettian tools. Previous work by one of the authors (BM) also documented possible adhesives on two additional tools (artifact A – Gravettian; artifact B – Protoaurignacian), potentially consisting of mixtures of organic and mineral materials, although further analyses are needed for confirmation.

Although the limited number of adhesive residues and their broad chemical characterisation prevented a detailed comparison of Neanderthal and AMH hafting traditions at Morín Cave, the careful application of a multi-analytical protocol enabled the identification of potential adhesives across multiple technocomplexes. These findings provide new insights into Palaeolithic adhesive technology and highlight the importance of integrating contextual information on artifact deposition and curation history, microscopic analysis, and multiple chemical residue characterisation methods for the accurate study of prehistoric organic materials.

Supplementary Information The online version contains supplementary material available at https://doi.org/10.1007/s41982-025-00251-0.

Acknowledgements The study of the material was permitted by the Gobierno de Cantabria, Consejería de Universidades, Igualdad, Cultura y Deporte, under the permits (resoluciónes) 340-21, 027-22 and 028-22. We are very thankful to the director and staff of the Museo de Prehistoria y Arqueología de Cantabria (MUPAC), in particular to R. Ontañón and A. Chauvin, for allowing us to study the material and for their collaboration and assistance during the research. We thank Prof J. Setién and Dr A. Cimentada of the LADICIM (University of Cantabria) for the SEM analysis. We are thankful to Prof A. van Gijn (Leiden University) for her help sorting the collection in Santander and to M. Baillet for his feedback during the initial stage of the research. Lastly, we are grateful to M. Fernández García and G. Terlato for the help and support during data collection in Santander.

Author Contributions A.A.: Conceptualization, Investigation, Formal Analysis, Writing – Original Draft, Writing – Review & Editing, Visualization; M.B.: Writing – Review & Editing; R.C.: Investigation, Formal Analysis, Writing – Review & Editing, Visualization; M.D.: Formal Analysis, Writing – Review & Editing; L.F.: Formal Analysis, Writing – Review & Editing, Visualization; J.G.: Formal Analysis, Writing – Review & Editing; P.K.: Investigation, Formal Analysis, Writing – Review & Editing, Visualization; F.R.: Formal Analysis, Writing – Review & Editing; G.L.: Conceptualization, Writing – Review & Editing, Funding Acquisition.

Funding This project has received funding from the European Research Council (ERC) under the European Union's Horizon 2020 Research and Innovation Programme, grant agreement number 804151. The funders had no role in study design, data collection and analysis, decision to publish, or preparation of the manuscript.

Data Availability Raw data of elemental and molecular analyses (SEM-EDX, Raman, ATR-FTIR, and GC-MS) were made available at 4TU.ResearchData. DOI: 10.4121/fc28fa90-cba2-485a-9221-033be73a0e04.

Declarations

Competing Interests The authors declare no competing interests.

References

Aleo, A., Duches, R., Falcucci, A., Rots, V., & Peresani, M. (2021). Scraping hide in the early upper paleolithic: Insights into the life and function of the protoaurignacian endscrapers at fumane cave. *Archaeological and Anthropological Sciences, 13*(8), 137. https://doi.org/10.1007/s12520-021-01367-4

Aleo, A., Kozowyk, P. R. B., Baron, L. I., van Gijn, A., & Langejans, G. H. J. (2023). The dynamic lives of osseous points from late Palaeolithic/Early mesolithic doggerland: A detailed functional study of barbed and unbarbed points from the Dutch North sea. *PLoS One*, *18*(8), e0288629. https://doi.org/10.1371/journal.pone.0288629

Aleo, A., Jerardino, A., Chasan, R., Despotopoulou, M., Ngan-Tillard, D., Hendrikx, R. W. A., & Langejans, G. H. J. (2024). A multi-analytical approach reveals flexible compound adhesive technology at Steenbokfontein Cave, Western Cape. *Journal of Archaeological Science*. https://doi.org/10.1016/j.jas.2024.105997

Aleo, A., Bradtmöller, M., Chasan, R., Despotopoulou, M., Gonzalez Gomez, J. A., Kozowyk, P. R. B., Gómez Fernández, L., Rodríguez, F., & Langejans, G. H. J. (2025). Raw data of molecular analyses (SEM-EDX, ATR-FTIR, Raman, and GC-MS) of adhesive residues from Morín Cave (Spain) Version 2). https://doi.org/10.4121/fc28fa90-cba2-485a-9221-033be73a0e04.v2

Allué, E., Martínez-Moreno, J., Roy, M., Benito-Calvo, A., & Mora, R. (2018). Montane pine forests in NE Iberia during MIS 3 and MIS 2. A study based on new anthracological evidence from Cova Gran (Santa Linya, Iberian Pre-Pyrenees). *Review of Palaeobotany and Palynology*, *258*, 62–72. https://doi.org/10.1016/j.revpalbo.2018.06.012

Arrizabalaga, Á., & Iriarte, M. J. (2006). El Castelperroniense y otros complejos de transición entre el Paleolítico medio y el superior en la Cornisa Cantábrica. Algunas reflexiones. In J.-M. Maíllo-Fernández & E. Baquedano (Eds.), *Miscelánea en homenaje a Victoria Cabrera. Zona Arqueológica, 7* (Vol. I, pp. 358–371).

Asquier, M., Colomban, P., & Milande, V. (2009). Raman and infrared analysis of glues used for pottery conservation treatments. *Journal of Raman Spectroscopy*, *40*(11), 1641–1644. https://doi.org/10.1002/jrs.2312

Baales, M., Birker, S., & Mucha, F. (2017). Hafting with beeswax in the final palaeolithic: A barbed point from Bergkamen. *Antiquity*, *91*(359), 1155–1170. https://doi.org/10.15184/aqy.2017.142

Badal, E., Bonilla, V., & Zilhão, J. (2011). The fire of Iberian Neanderthals. Wood charcoal from three new Mousterian sites in the Iberian Peninsula.

Bickford, M. E., & Basu, A. (2023). *Dickinsonia tenuis* reported by Retallack et al. 2021 is not a fossil, instead an impression of an extant 'fallen beehive' by S.K. Pandey, Shamim Ahmad and Mukund Sharma. Jour. Geol. Soc. India, v.99, 2023, pp.311–316. *Journal of the Geological Society of India, 99*(7), 1033–1036. https://doi.org/10.1007/s12594-023-2427-5

Birkemeyer, C. S., Thomsen, R., Jänig, S., Kücklich, M., Slama, A., Weiß, B. M., & Widdig, A. (2016). Sampling the body odor of primates: Cotton swabs sample semivolatiles rather than volatiles. *Chemical Senses, 41*(6), 525–535. https://doi.org/10.1093/chemse/bjw056

Blomquist, G. J., & Jackson, L. L. (1979). Chemistry and biochemistry of insect waxes. *Progress in Lipid Research*, *17*(4), 319–345. https://doi.org/10.1016/0079-6832(79)90011-9

Boëda, E., Bonilauri, S., Connan, J., Jarvie, D., Mercier, N., Tobey, M., Valladas, H., & Al-Sakhel, H. (2008a). New evidence for significant use of bitumen in Middle Palaeolithic technical systems at Umm el Tlel (Syria) around 70,000 BP. *Paléorient, 34*(2), 67–83. https://doi.org/10.3406/paleo.2008.5257

Boëda, E., Bonilauri, S., Connan, J., Jarvie, D., Mercier, N., Tobey, M., Valladas, H., Al-Sakhel, H., & Muhesen, S. (2008b). Middle palaeolithic bitumen use at Umm El Tlel around 70 000 BP. *Antiquity*, *82*(318), 853–861. https://doi.org/10.1017/S0003598X00097623

Bordes, L., Prinsloo, L. C., Fullagar, R., Sutikna, T., Hayes, E., Jatmiko, W., Saptomo, E., Tocheri, M. W., & Roberts, R. G. (2017). Viability of Raman microscopy to identify micro-residues related to tool-use and modern contaminants on prehistoric stone artefacts. *Journal of Raman Spectroscopy*, *48*(9), 1212–1221. https://doi.org/10.1002/jrs.5202

Bradtmöller, M., Sarmiento, A., Perales, U., & Zuluaga, M. C. (2016). Investigation of upper palaeolithic adhesive residues from Cueva Morín, Northern Spain. *Journal of Archaeological Science: Reports*, *7*, 1–13. https://doi.org/10.1016/j.jasrep.2016.03.051

Bray, E. E., & Evans, E. D. (1961). Distribution of n-paraffins as a clue to recognition of source beds. *Geochimica et Cosmochimica Acta, 22*(1), 2–15. https://doi.org/10.1016/0016-7037(61)90069-2

Brody, R. H., Edwards, H. G. M., & Pollard, A. M. (2002). Fourier transform-Raman spectroscopic study of natural resins of archaeological interest [Article]. *Biopolymers - Biospectroscopy Section, 67*(2), 129–141. https://doi.org/10.1002/bip.10059

Bush, R. T., & McInerney, F. A. (2013). Leaf wax n-alkane distributions in and across modern plants: Implications for paleoecology and chemotaxonomy. *Geochimica et Cosmochimica Acta, 117*, 161–179. https://doi.org/10.1016/j.gca.2013.04.016

Cabrera, V., Arrizabalaga, Á., de Quirós Guidotti, F. B., & Maíllo-Fernández, J. M. (2004). *La transición al Paleolítico superior y La evolución de Los contextos auriñacienses (50.000–27.000 BP)*. Las sociedades del Paleolítico en la región cantábrica.

Carballo, J. (1923). *Excavaciones en la cueva del Rey en Villanueva (Santander)*.

Cârciumaru, M., Ion, R. M., Niţu, E. C., & Ştefănescu, R. (2012). New evidence of adhesive as hafting material on middle and upper palaeolithic artefacts from Gura Cheii-Râşnov cave (Romania).

Journal of Archaeological Science, *39*(7), 1942–1950. https://doi.org/10.1016/j.jas.2012.02.016

Chen, S., Vahur, S., Teearu, A., Juus, T., Zhilin, M., Savchenko, S., Oshibkina, S., Asheichyk, V., Vashanau, A., Lychagina, E., Kashina, E., German, K., Dubovtseva, E., Kriiska, A., Leito, I., & Oras, E. (2022). Classification of archaeological adhesives from Eastern Europe and Urals by ATR-FT-IR spectroscopy and chemometric analysis [doi: 10.1111/arcm.12686]. *Archaeometry, 64*(1), 227–244.

Cleland, T. P., & Schroeter, E. R. (2018). A comparison of common mass spectrometry approaches for paleoproteomics. *Journal of Proteome Research*, *17*(3), 936–945. https://doi.org/10.1021/acs.jproteome.7b00703

Cnuts, D., & Rots, V. (2017). Extracting residues from stone tools for optical analysis: Towards an experiment-based protocol. *Archaeological and Anthropological Sciences*, *10*(7), 1717–1736. https://doi.org/10.1007/s12520-017-0484-7

Coppe, J., & Rots, V. (2017). Focus on the target. The importance of a transparent fracture terminology for understanding projectile points and projecting modes. *Journal of Archaeological Science: Reports, 12*, 109–123. https://doi.org/10.1016/j.jasrep.2017.01.010

Coppe, J., & Rots, V. (2025). Let's cut to the chase and rely on fracture mechanics to identify projectile armatures. *Archaeological and Anthropological Sciences, 17*(3), 73. https://doi.org/10.1007/s12520-025-02180-z

Covi-Schwarz, J., Klang, V., & Valenta, C. (2017). ATR-FTIR Spectroscopy and the Skin Barrier: Evaluation of Penetration-Enhancement Effects. In N. Dragicevic & H. I. Maibach (Eds.), *Percutaneous Penetration Enhancers Drug Penetration Into/Through the Skin: Methodology and General Considerations* (pp. 247–254). Springer Berlin Heidelberg. https://doi.org/10.1007/978-3-662-53270-6_14

Croft, S., Chatzipanagis, K., Kröger, R., & Milner, N. (2018). Misleading residues on lithics from star carr: Identification with Raman microspectroscopy. *Journal of Archaeological Science: Reports*, *19*, 430–438. https://doi.org/10.1016/j.jasrep.2018.03.018

Daher, C., Paris, C., Hô, L., Bellot-Gurlet, A. S., L., & Échard, J. P. (2010). A joint use of Raman and infrared spectroscopies for the identification of natural organic media used in ancient varnishes. *Journal of Raman Spectroscopy*, *41*(11), 1494–1499. https://doi.org/10.1002/jrs.2693

David, I. G., Popa, D.-E., & Buleandra, M. (2017). Pencil graphite electrodes: A versatile tool in electroanalysis. *Journal of Analytical Methods in Chemistry, 2017*, Article 1905968. https://doi.org/10.1155/2017/1905968

Dayet, L., d'Errico, F., & Garcia-Moreno, R. (2014). Searching for consistencies in Châtelperronian pigment use. *Journal of Archaeological Science*, *44*, 180–193. https://doi.org/10.1016/j.jas.2014.01.032

Dayet, L., Faivre, J.-P., Le Bourdonnec, F.-X., Discamps, E., Royer, A., Claud, E., Lahaye, C., Cantin, N., Tartar, E., Queffelec, A., Gravina, B., Turq, A., & d'Errico, F. (2019). Manganese and iron oxide use at Combe-Grenal (Dordogne, France): A proxy for cultural change in Neanderthal communities. *Journal of Archaeological Science: Reports, 25*, 239–256. https://doi.org/10.1016/j.jasrep.2019.03.027

Degano, I., Soriano, S., Villa, P., Pollarolo, L., Lucejko, J. J., Jacobs, Z., Douka, K., Vitagliano, S., & Tozzi, C. (2019). Hafting of middle paleolithic tools in Latium (central Italy): New data from Fossellone and sant'agostino caves. *PLoS One*, *14*(6), e0213473. https://doi.org/10.1371/journal.pone.0213473

Despotopoulou, M. (2022). *Testing non-destructive analysis for archaeological adhesives*. Delft University of Technology].

Despotopoulou, M., Langejans, G. H. J., Hendrikx, R. W. A., Joosten, I., Nijemeisland, M., Poulis, J. A., & Kozowyk, P. R. B. (2024). Testing non-destructive spectrometric methods for the identification and distinction of archaeological pine wood tar and birch bark tar. *Journal of Archaeological Science: Reports, 56*, 104571. https://doi.org/10.1016/j.jasrep.2024.104571

Dinnis, R., Pawlik, A., & Gaillard, C. (2009). Bladelet cores as weapon tips? Hafting residue identification and micro-wear analysis of three carinated burins from the late aurignacian of les Vachons, France. *Journal of Archaeological Science*, *36*(9), 1922–1934. https://doi.org/10.1016/j.jas.2009.04.020

Doronicheva, E. V., Golovanova, L. V., Kostina, J. V., Legkov, S. A., Poplevko, G. N., Revina, E. I., Rusakova, O. Y., & Doronichev, V. B. (2022). Functional characterization of mousterian tools from the Caucasus using comprehensive use-wear and residue analysis. *Scientific Reports*, *12*(1), 17421. https://doi.org/10.1038/s41598-022-20612-x

Echegaray, J. G., Freeman, L. G., Butzer, K. W., Leroi-Gourhan, A., Altuna, J., Madariaga, B., & Apellániz, J. (1971). (P. d. l. C. P. d. l. P. d. Santander, Ed). *Cueva morin: excavaciones, 1966–1968*. Aldus Velarde SA.

Edwards, H. G. M., & Ali, E. M. A. (2011). Raman spectroscopy of archaeological and ancient resins: Problems with database construction for applications in conservation and historical provenancing. *Spectrochimica Acta Part A: Molecular and Biomolecular Spectroscopy*, *80*(1), 49–54. https://doi.org/10.1016/j.saa.2011.01.030

Edwards, H. G. M., Farwell, D. W., & Daffner, L. (1996). Fourier-transform Raman spectroscopic study of natural waxes and resins. I. *Spectrochimica Acta Part A: Molecular and Biomolecular Spectroscopy*, *52*(12), 1639–1648. https://doi.org/10.1016/0584-8539(96)01730-8

Evershed, R. P. (2008). Organic residue analysis in archaeology: The Archaeological Biomarker Revolution. *Archaeometry, 50*(6), 895–924. https://doi.org/10.1111/j.1475-4754.2008.00446.x

Fajardo, S., Kozowyk, P. R. B., & Langejans, G. H. L. (2023). Measuring ancient technological complexity and its cognitive implications using petri Nets. *Scientific Reports*. https://doi.org/10.1038/s41598-023-42078-1

Fernández-García, M., Vidal-Cordasco, M., Jones, J. R., & Marín-Arroyo, A. B. (2023). Reassessing palaeoenvironmental conditions during the middle to upper palaeolithic transition in the Cantabrian region (Southwestern Europe). *Quaternary Science Reviews*, *301*, 107928. https://doi.org/10.1016/j.quascirev.2022.107928

Fischer, A., Hansen, P. V., & Rasmussen, P. (1984). Macro and micro wear traces on lithic projectile points: Experimental results and prehistoric examples. *Journal of Danish Archaeology*, *3*(1), 19–46.

Frade, J. C., Soares, A. M., Candeias, A., Ribeiro, M. I. M., Ponte, T., Serra, M., & Porfírio, E. (2014). Beeswax and propolis as sealants of funerary chambers during the Middle Bronze Age in the South-Western Iberian Peninsula. Proceedings of the 39th International Symposium for Archaeometry, Centre for Archaeological Science.

Frahm, E., Adler, D. S., Gasparyan, B., Luo, B., Mallol, C., Pajović, G., Tostevin, G. B., Yeritsyan, B., & Monnier, G. (2022). Every contact leaves a trace: Documenting contamination in lithic residue studies at the middle palaeolithic sites of Lusakert cave 1 (Armenia) and Crvena Stijena (Montenegro). *PLoS One*, *17*(4), e0266362. https://doi.org/10.1371/journal.pone.0266362

Fullagar, R. (2006). Residues and usewear. In J. Balme & A. Paterson (Eds.), *Archaeology in Practice. A Student Guide to Archaeological Analyses* (pp. 207–233). Blackwell Publishing.

Gauquelin, T., Bertaudiere, V., Montes, N., Badri, W., & Asmode, J. (1999). Endangered stands of thuriferous Juniper in the Western mediterranean basin: Ecological status, conservation and management. *Biodiversity and Conservation, 8*(11), 1479–1498. https://doi.org/10.1023/A:1008966808796

Gibson, N. E., Wadley, L., & Williamson, B. S. (2004). Microscopic residues as evidence of hafting on backed tools from the 60 000 to 68 000 year-old Howiesons Poort layers of Rose Cottage Cave, South Africa. *Southern African Humanities, 16*, 1–11.

Hanesch, M. (2009). Raman spectroscopy of iron oxides and (oxy) hydroxides at low laser power and possible applications in environmental magnetic studies. *Geophysical Journal International*, *177*(3), 941–948. https://doi.org/10.1111/j.1365-246X.2009.04122.x

Hardy, K., Buckley, S., Collins, M. J., Estalrrich, A., Brothwell, D., Copeland, L., García-Tabernero, A., García-Vargas, S., de la Rasilla, M., Lalueza-Fox, C., Huguet, R., Bastir, M., Santamaría, D., Madella, M., Wilson, J., Cortés, Á. F., & Rosas, A. (2012). Neanderthal medics? Evidence for food, cooking, and medicinal plants entrapped in dental calculus. *Naturwissenschaften*, *99*(8), 617–626. https://doi.org/10.1007/s00114-012-0942-0

Hauck, T. C., Connan, J., Charrié-Duhaut, A., Le Tensorer, J.-M., & al Sakhel, H. (2013). Molecular evidence of bitumen in the Mousterian lithic assemblage of Hummal (Central Syria). *Journal of Archaeological Science, 40*(8), 3252–3262. https://doi.org/10.1016/j.jas.2013.03.022

Hayes, E., & Rots, V. (2019). Documenting scarce and fragmented residues on stone tools: An experimental approach using optical microscopy and SEM-EDS. *Archaeological and Anthropological Sciences, 11*(7), 3065–3099. https://doi.org/10.1007/s12520-018-0736-1

Hazen, R. M. (1988). High-Pressure Research in Mineral Physics. *Eos, Transactions American Geophysical Union, 69*(39), 875–882. https://doi.org/10.1029/88EO01136

Hershkovitz, I., Weber, G. W., Quam, R., Duval, M., Grün, R., Kinsley, L., Ayalon, A., Bar-Matthews, M., Valladas, H., Mercier, N., Arsuaga, J. L., Martinón-Torres, M., Bermúdez de Castro, J. M., Fornai, C., Martín-Francés, L., Sarig, R., May, H., Krenn, V. A., Slon, V., Rodríguez, L., García, R., Lorenzo, C., Carretero, J. M., Frumkin, A., Shahack-Gross, R., Bar-Yosef Mayer, D. E., Cui, Y., Wu, X., Peled, N., Groman-Yaroslavski, I., Weissbrod, L., Yeshurun, R., Tsatskin, A., Zaidner, Y., & Weinstein-Evron, M. (2018). The earliest modern humans outside Africa. *Science*, *359*(6374), 456–459. https://doi.org/10.1126/science.aap8369

Jones, J. R., Richards, M. P., Reade, H., Bernaldo de Quirós, F., & Marín-Arroyo, A. B. (2019). Multi-Isotope investigations of ungulate bones and teeth from El Castillo and Covalejos caves (Cantabria, Spain): Implications for paleoenvironment reconstructions across the Middle-Upper palaeolithic transition. *Journal of Archaeological Science: Reports*, *23*, 1029–1042. https://doi.org/10.1016/j.jasrep.2018.04.014

Keeley, L. H. (1980). *Experimental Determination of Stone Tool Uses: A Microwear Analysis*. University of Chicago Press.

Koller, J., Baumer, U., & Mania, D. (2001). High-tech in the middle palaeolithic: Neandertal-Manufactured pitch identified. *European Journal of Archaeology, 4*(3), 385–397. https://doi.org/10.1177/146195710100400315

Kozowyk, P. R. B., Langejans, G. H. J., & Poulis, J. A. (2016). Lap shear and impact testing of ochre and beeswax in experimental middle stone age compound adhesives. *PLoS One*, *11*(3), e0150436. https://doi.org/10.1371/journal.pone.0150436

Kozowyk, P. R. B., Soressi, M., Pomstra, D., & Langejans, G. H. J. (2017). Experimental methods for the palaeolithic dry distillation of Birch bark: Implications for the origin and development of neandertal adhesive technology. *Scientific Reports*, *7*(1), 8033. https://doi.org/10.1038/s41598-017-08106-7

Kozowyk, P. R. B., Fajardo, S., & Langejans, G. H. J. (2023). Scaling palaeolithic Tar production processes exponentially increases behavioural complexity. *Scientific Reports*, *13*(1), 14709. https://doi.org/10.1038/s41598-023-41963-z

Kruge, M. A., & Suárez-Ruiz, I. (1991). Organic geochemistry and petrography of Spanish oil shales. *Fuel*, *70*(11), 1298–1302. https://doi.org/10.1016/0016-2361(91)90217-X

Langejans, G. H. J., & Lombard, M. (2015). About Small Things and Bigger Pictures: An Introduction to the Morphological Identification of Micro-Residues on Stone Tools. In J. Marreiros, M. Gibaja Bao, J. F. Ferreira, & N. Bicho (Eds.), *Use-Wear and Residue Analysis in Archaeology* (pp. 199–219). Springer.

Langejans, G., Aleo, A., Fajardo, S., & Kozowyk, P. (2022). Archaeological adhesives. *Oxford Research Encyclopedia of Anthropology*. https://doi.org/10.1093/acrefore/9780190854584.013.198

Langejans, G. H. J., Pomstra, D., Ducrocq, T., Haskins, A., & Kozowyk, P. R. B. (2023). Conifer tar in the late Upper Palaeolithic and Mesolithic of north-western Europe. *Analecta Praehistorica Leidensia*, *In Press*.

Leroi-Gourhan, A. (1971). Analisis polínico de cueva Morín. In J. González Echegaray & L. Freeman (Eds.), *Cueva Morín: Excavaciones 1966–1968* (pp. 359–365).

Lombard, M. (2006). Direct evidence for the use of ochre in the hafting technology of middle stone age tools from Sibudu cave. *Southern Africa Humanities*, *18*(1), 57–67.

Lombard, M. (2008). Finding resolution for the Howiesons Poort through the microscope: Micro-residue analysis of segments from Sibudu Cave, South Africa. *Journal of Archaeological Science, 35*(1), 26–41. https://doi.org/10.1016/j.jas.2007.02.021

Lombard, M., & Wadley, L. (2007). The morphological identification of micro-residues on stone tools using light microscopy: Progress and difficulties based on blind tests. *Journal of Archaeological Science*, *34*(1), 155–165. https://doi.org/10.1016/j.jas.2006.04.008

Maíllo-Fernández, J.-M. (2005). La producción laminar en el Chatelperroniense de Cueva Morín: Modalidades, intenciones y objetivos. *Trabajos de Prehistoria, 62*(1), 47–64.

Maíllo-Fernández, J.-M. (2006). Archaic Aurignacian lithic technology in Cueva Morín (Cantabria, Spain). In O. Bar-Yosef & J. Zilhão (Eds.), *Towards a Definition of the Aurignacian* (pp. 109–128). IPA.

Maíllo-Fernández, J. M. (2012). Missing lithics: the role of flakes in the Early Upper Palaeolithic of the Cantabrian Region (Spain). In A. Pastoors & M. Peresani (Eds.), *Flakes Not Blades: The Role of Flake Production at the Onset of the Upper Palaeolithic in Europe* (Vol. 5, 69–84).

Maíllo-Fernández, J.-M.M., Valladas, H., Cabrera Valdés, V., & de Bernardo Quirós, F. (2001). Nuevas dataciones para el Paleolítico superior de Cueva Morín (Villanueva de Villaescusa, Cantabria). *Espacio, Tiempo y Forma. Serie I, Prehistoria y Arqueología, 14*, 145–150.

Maíllo-Fernández, J.-M., Arteaga, C., Iriarte-Chiapusso, M.-J., Fernández, A., Wood, R., & Quirós, F. (2014). Cueva Morín (Villanueva de Villaescusa, Cantabria). In R. Sala Ramos (Ed.), *Pleistocene and Holocene hunter-gatherers in Iberia and the Gibraltar Strait: The current archaeological record* (pp. 72–78). Universidad de Burgos.

Marín-Arroyo, A. B., Rios-Garaizar, J., Straus, L. G., Jones, J. R., de la Rasilla, M., González Morales, M. R., Richards, M., Altuna, J., Mariezkurrena, K., & Ocio, D. (2018). Chronological reassessment of the middle to upper paleolithic transition and early upper paleolithic cultures in Cantabrian Spain. *PLoS One*, *13*(4), e0194708. https://doi.org/10.1371/journal.pone.0194708

Mazza, P. P. A., Martini, F., Sala, B., Magi, M., Colombini, M. P., Giachi, G., Landucci, F., Lemorini, C., Modugno, F., & Ribechini, E. (2006). A new palaeolithic discovery: Tar-Hafted stone tools in a European Mid-Pleistocene Bone-Bearing bed. *Journal of Archaeological Science*, *33*(9), 1310–1318. https://doi.org/10.1016/j.jas.2006.01.006

Metz, L., Lewis, J. E., & Slimak, L. (2023). Bow-and-arrow, technology of the first modern humans in Europe 54,000 years ago at Mandrin, France. *Science Advances*, *9*(8), eadd4675. https://doi.org/10.1126/sciadv.add4675

Monnier, G., & May, K. (2019). Documenting the degradation of animal-tissue residues on experimental stone tools: A multi-analytical approach. *Archaeological and Anthropological Sciences*, *11*(12), 6803–6827. https://doi.org/10.1007/s12520-019-00941-1

Monnier, G. F., Hauck, T. C., Feinberg, J. M., Luo, B., Tensorer, L., J.-M.,al, & Sakhel, H. (2013). A multi-analytical methodology of lithic residue analysis applied to paleolithic tools from Hummal, Syria. *Journal of Archaeological Science*, *40*(10), 3722–3739. https://doi.org/10.1016/j.jas.2013.03.018

Monnier, G., Frahm, E., Luo, B., & Missal, K. (2017). Developing FTIR microspectroscopy for analysis of plant residues on stone tools. *Journal of Archaeological Science*, *78*, 158–178. https://doi.org/10.1016/j.jas.2016.12.004

Monnier, G., Frahm, E., Luo, B., & Missal, K. (2018). Developing FTIR microspectroscopy for the analysis of animal-tissue residues on stone tools. *Journal of Archaeological Method and Theory, 25*(1), 1–44. https://doi.org/10.1007/s10816-017-9325-3

Namdar, D., Neumann, R., Sladezki, Y., Haddad, N., & Weiner, S. (2007). Alkane composition variations between darker and lighter colored comb beeswax. *Apidologie*, *38*(5), 453–461. https://doi.org/10.1051/apido:2007033

Nardella, F., Duce, C., & Ribechini, E. (2021). Analytical pyrolysis and thermal analysis to chemically characterise bitumen from Italian geological deposits and neolithic stone tools. *Journal of Analytical and Applied Pyrolysis*, *158*, 105262. https://doi.org/10.1016/j.jaap.2021.105262

Niekus, M., Kozowyk, P. R. B., Langejans, G. H. J., Ngan-Tillard, D., van Keulen, H., van der Plicht, J., Cohen, K. M., van Wingerden, W., van Os, B., Smit, B. I., Amkreutz, L., Johansen, L., Verbaas, A., & Dusseldorp, G. L. (2019). Middle paleolithic complex technology and a neandertal tar-backed tool from the Dutch North sea. *Proc Natl Acad Sci U S A*, *116*(44), 22081–22087. https://doi.org/10.1073/pnas.1907828116

Obermaier, H. (1916). El hombre Fósil. Museo Nacional de Ciencias Naturales. In *Comisión de Investigaciones Paleontológicas y Prehistóricas* (Vol. 9).

Ochando, J., Amorós, G., Carrión, J. S., Fernández, S., Munuera, M., Camuera, J., Jiménez-Moreno, G., González-Sampériz, P., Burjachs, F., Marín-Arroyo, A. B., Roksandic, M., & Finlayson, C. (2022). Iberian neanderthals in forests and savannahs. *Journal of Quaternary Science*, *37*(2), 335–362. https://doi.org/10.1002/jqs.3339

Olsztyńska-Janus, S., Pietruszka, A., Kiełbowicz, Z., & Czarnecki, M. A. (2018). ATR-IR study of skin components: Lipids, proteins and water. Part I: Temperature effect. *Spectrochimica Acta Part A: Molecular and Biomolecular Spectroscopy*, *188*, 37–49. https://doi.org/10.1016/j.saa.2017.07.001

Pärnpuu, S., Astover, A., Tõnutare, T., Penu, P., & Kauer, K. (2022). Soil organic matter qualification with FTIR spectroscopy under different soil types in Estonia. *Geoderma Regional*, *28*, e00483. https://doi.org/10.1016/j.geodrs.2022.e00483

Parras, D. J., Sánchez, A., Tuñón, J. A., Rueda, C., Ramos, N., & García-Reyes, J. F. (2015). Sulphur, fats and beeswax in the Iberian rites of the sanctuary of the oppidum of Puente Tablas (Jaén, Spain). *Journal of Archaeological Science: Reports*, *4*, 510–524. https://doi.org/10.1016/j.jasrep.2015.10.010

Pasieczna-Patkowska, S., Cichy, M., & Flieger, J. (2025). Application of Fourier transform infrared (FTIR) spectroscopy in characterization of green synthesized nanoparticles. *Molecules*. https://doi.org/10.3390/molecules30030684

Pawlik, A. F., & Thissen, J. P. (2011). Hafted armatures and multicomponent tool design at the Micoquian site of Inden-Altdorf, Germany. *Journal of Archaeological Science*, *38*(7), 1699–1708. https://doi.org/10.1016/j.jas.2011.03.001

Pedergnana, A., Asryan, L., Fernández-Marchena, J. L., & Ollé, A. (2016). Modern contaminants affecting microscopic residue analysis on stone tools: A word of caution. *Micron (Oxford, England : 1993)*, *86*, 1–21. https://doi.org/10.1016/j.micron.2016.04.003

Polla, S., & Springer, A. (2022). Organic Residues Analysis (ORA) in Archaeology. In S. D'Amico & V. Venuti (Eds.), *Handbook of Cultural Heritage Analysis* (pp. 1075–1119). Springer International Publishing. https://doi.org/10.1007/978-3-030-60016-7_37

Prinsloo, L. C., Tournié, A., Colomban, P., Paris, C., & Bassett, S. T. (2013). In search of the optimum Raman/IR signatures of potential ingredients used in San/Bushman rock Art paint. *Journal of Archaeological Science*, *40*(7), 2981–2990. https://doi.org/10.1016/j.jas.2013.02.010

Prinsloo, L. C., Bordes, L., Mauran, G., Lombard, M., & Wadley, L. (2023). Graphite and multilayer graphene detected on ~70,000-year-old stone tools: Geological origin or constituent. *Journal of Raman Spectroscopy*, *54*(2), 182–190. https://doi.org/10.1002/jrs.6474

Radini, A., Buckley, S., Rosas, A., Estalrrich, A., de la Rasilla, M., & Hardy, K. (2016). Neanderthals, trees and dental calculus: New evidence from El Sidrón. *Antiquity*, *90*(350), 290–301. https://doi.org/10.15184/aqy.2016.21

Radini, A., Nikita, E., Buckley, S., Copeland, L., & Hardy, K. (2017). Beyond food: The multiple pathways for inclusion of materials into ancient dental calculus. *American Journal of Physical Anthropology*, *162*(S63), 71–83. https://doi.org/10.1002/ajpa.23147

Randolph-Quinney, P. S., Backwell, L. R., Berger, L. R., Hawks, J., Dirks, P. H. G. M., Roberts, E. M., Nhauro, G., & Kramers, J. (2016). Response to Thackeray (2016) - The possibility of lichen growth on bones of *Homo naledi*: Were they exposed to light? *South African Journal of Science, 112*, 1–5.

Regert, M., Alexandre, V., Thomas, N., & Lattuati-Derieux, A. (2006). Molecular characterisation of birch bark tar by headspace solid-phase microextraction gas chromatography–mass spectrometry: A new way for identifying archaeological glues. *Journal of Chromatography A, 1101*(1–2), 245–253. https://doi.org/10.1016/j.chroma.2005.09.070

Rime, M.-J., Ali, T., Jean, B., & Arlette, B.-G. (2011). Chemometric approach for investigating the skin surface lipids (SSLs) composition: Influence of geographical localization. *European Journal of Dermatology, 21*(2), 63–71. https://doi.org/10.1684/ejd.2011.1263

Roebroeks, W., & Soressi, M. (2016). Neandertals revised. *Proceedings of the National Academy of Sciences of the United States of America*, *113*(23), 6372–6379. https://doi.org/10.1073/pnas.1521269113

Roebroeks, W., Sier, M. J., Nielsen, T. K., De Loecker, D., Parés, J. M., Arps, C. E. S., & Mücher, H. J. (2012). Use of red ochre by early Neandertals. *Proceedings of the National Academy of Sciences, 109*(6), 1889–1894. https://doi.org/10.1073/pnas.1112261109

Rots, V. (2010). Prehension and hafting traces on flint tools: a methodology.

Rots, V. (2016). Projectiles and Hafting Technology. In R. Iovita & K. Sano (Eds.), *Multidisciplinary Approaches to the Study of Stone Age Weaponry* (pp. 167–185). Springer Netherlands. https://doi.org/10.1007/978-94-017-7602-8_12

Rots, V., & Plisson, H. (2014). Projectiles and the abuse of the use-wear method in a search for impact. *Journal of Archaeological Science*, *48*, 154–165. https://doi.org/10.1016/j.jas.2013.10.027

Rots, V., Van Peer, P., & Vermeersch, P. M. (2011). Aspects of tool production, use, and hafting in palaeolithic assemblages from Northeast Africa. *Journal of Human Evolution*, *60*(5), 637–664. https://doi.org/10.1016/j.jhevol.2011.01.001

Rots, V., Cnuts, D., Coppe, J., Lokker, A., & Oberholzer, R. (2024). No solid foundation for the use of ochre-based compound adhesives at Le moustier. *Journal of Paleolithic Archaeology, 7*(1), 32. https://doi.org/10.1007/s41982-024-00197-9

Roussel, M., Soressi, M., & Hublin, J. J. (2016). The Châtelperronian conundrum: Blade and bladelet lithic technologies from Quinçay, France. *Journal of Human Evolution*, *95*, 13–32. https://doi.org/10.1016/j.jhevol.2016.02.003

Sanguino, J., Montes-Barquín, R., & Blanco, P. (2005). El marco cronoestratigráfico y paleoclimático del Pleistoceno superior inicial de la región cantábrica, ¿un gigante con pies de barro? *Geoarqueología y Patrimonio en la Península Ibérica y el entorno mediterráneo*, 127–138.

Sano, K., Arrighi, S., Stani, C., Aureli, D., Boschin, F., Fiore, I., Spagnolo, V., Ricci, S., Crezzini, J., Boscato, P., Gala, M., Tagliacozzo, A., Birarda, G., Vaccari, L., Ronchitelli, A., Moroni, A., & Benazzi, S. (2019). The earliest evidence for mechanically delivered projectile weapons in Europe. *Nature Ecology & Evolution, 3*(10), 1409–1414. https://doi.org/10.1038/s41559-019-0990-3

Scalan, E. S., & Smith, J. E. (1970). An improved measure of the odd-even predominance in the normal alkanes of sediment extracts and petroleum. *Geochimica et Cosmochimica Acta, 34*(5), 611–620. https://doi.org/10.1016/0016-7037(70)90019-0

Schmidt, P., Blessing, M., Rageot, M., Iovita, R., Pfleging, J., Nickel, K. G., Righetti, L., & Tennie, C. (2019). Birch tar production does not prove neanderthal behavioral complexity. *Proceedings of the National Academy of Sciences of the United States of America, 116*(36), 17707–17711. https://doi.org/10.1073/pnas.1911137116

Schmidt, P., Koch, T. J., Blessing, M. A., Karakostis, F. A., Harvati, K., Dresely, V., & Charrié-Duhaut, A. (2023). Production method of the Königsaue Birch Tar documents cumulative culture in neanderthals. *Archaeological and Anthropological Sciences*, *15*(6), 84. https://doi.org/10.1007/s12520-023-01789-2

Schmidt, P., Iovita, R., Charrié-Duhaut, A., Möller, G., Namen, A., & Dutkiewicz, E. (2024). Ochre-based compound adhesives at the mousterian type-site document complex cognition and high investment. *Science Advances*, *10*(8), eadl0822. https://doi.org/10.1126/sciadv.adl0822

Semenov, S. (1964). *Prehistoric technology: an experimental study of the oldest tools and artefacts from traces of manufacture and wear*. Cory, Adams & Mackay. (Pervobytnaja technika. Opyt izučenija drevnejših orudij i izdelij po sledam raboty (1957).

Serb, A. F., Georgescu, M., Onulov, R., Novaconi, C. R., Sisu, E., Bolocan, A., & Sandu, R. E. (2024). Mass-Spectrometry-Based research of cosmetic ingredients. *Molecules*, *29*(6), 1336. https://doi.org/10.3390/molecules29061336

Soriano, S., Villa, P., Delagnes, A., Degano, I., Pollarolo, L., Lucejko, J. J., Henshilwood, C., & Wadley, L. (2015). The still Bay and Howiesons Poort at Sibudu and blombos: Understanding middle stone age technologies. *PLoS One*, *10*(7), e0131127. https://doi.org/10.1371/journal.pone.0131127

Taipale, N., & Rots, V. (2020). Revisiting Maisières Canal (Hainaut, BE): New results on tool use and hafting. *Notae Praehistoricae, 40*(2020), 105–127.

Taipale, N., Chiotti, L., & Rots, V. (2022a). Why did hunting weapon design change at Abri pataud? Lithic use-wear data on armature use and hafting around 24,000–22,000 BP. *PLoS One*, *17*(1), e0262185. https://doi.org/10.1371/journal.pone.0262185

Taipale, N., Cnuts, D., Chiotti, L., Conard, N. J., & Rots, V. (2022b). What about apatite? Possibilities and limitations of recognising bone mineral residues on stone tools. *Journal of Paleolithic Archaeology*, *6*(1), 21. https://doi.org/10.1007/s41982-022-00132-w

Tinti, A., Tugnoli, V., Bonora, S., & Francioso, O. (2015). Recent applications of vibrational mid-Infrared (IR) spectroscopy for studying soil components: A review. *Journal of Central European Agriculture*, *16*(1), 0–0.

Tomasso, S., Cnuts, D., Coppe, J., Geerts, F., Van Gils, M., De Bie, M., & Rots, V. (2021). A closer look at an eroded dune landscape: First functional insights into the Federmessergruppen site of Lommel-Maatheide. *Peer Community Journal*. https://doi.org/10.24072/pcjournal.67

Traoré, M., Kaal, J., & Martínez Cortizas, A. (2018). Differentiation between pine woods according to species and growing location using FTIR-ATR. *Wood Science and Technology*, *52*(2), 487–504. https://doi.org/10.1007/s00226-017-0967-9

Tringham, R., Cooper, G., Odell, G., Voytek, B., & Whitman, A. (1974). Experimentation in the formation of edge damage: A new approach to lithic analysis. *Journal of Field Archaeology*, *1*(1–2), 171–196. https://doi.org/10.1179/jfa.1974.1.1-2.171

Tydgadt, L., & Rots, V. (2022). Stick to it! Mechanical performance tests to explore the resilience of prehistoric glues in hafting. *Archaeometry*,64(5), 1252–1269. https://doi.org/10.1111/arcm.12779

Vahur, S., Kriiska, A., & Leito, I. (2011). Investigation of the adhesive residue on the Flint insert and the adhesive lump found from the Pulli early mesolithic settlement site (Estonia) by micro-ATR-FT-IR spectroscopy. *Estonian Journal of Archaeology*, *15*(1), 3.

Van Gijn, A. L. (2010). *Flint in Focus. Lithic Biographies in the Neolithic and Bronze Age*. Sidestone Press.

Wadley, L. (2005). Putting ochre to the test: Replication studies of adhesives that may have been used for hafting tools in the Middle Stone Age. *Journal of Human Evolution, 49*(5), 587–601.

Wadley, L. (2010). Compound-adhesive manufacture as a behavioral proxy for complex cognition in the middle stone age. *Current Anthropology, 51*(S1), S111–S119. https://doi.org/10.1086/649836

Wadley, L. (2013). Recognizing complex cognition through innovative technology in stone age and palaeolithic sites. *Cambridge Archaeological Journal*, *23*(2), 163–183. https://doi.org/10.1017/S0959774313000309

Wadley, L., Hodgskiss, T., & Grant, M. (2009). Implications for complex cognition from the hafting of tools with compound adhesives in the middle stone Age, South Africa. *Proceedings of the National Academy of Sciences of the United States of America, 106*(24), 9590–9594. https://doi.org/10.1073/pnas.0900957106

Wesełucha-Birczyńska, A., Trąbska, J., & Oliva, M. (2012). Composition of a floor from an upper paleolithic skeletal grave – A case from Dolni vestonice (Moravia, Czechia, central Europe). *Vibrational Spectroscopy*, *60*, 129–132. https://doi.org/10.1016/j.vibspec.2011.11.013

Whelton, H. L., Hammann, S., Cramp, L. J. E., Dunne, J., Roffet-Salque, M., & Evershed, R. P. (2021). A call for caution in the analysis of lipids and other small biomolecules from archaeological contexts. *Journal of Archaeological Science*, *132*, 105397. https://doi.org/10.1016/j.jas.2021.105397

Wojcieszak, M., & Wadley, L. (2018). Raman spectroscopy and scanning electron microscopy confirm ochre residues on 71 000-year-old bifacial tools from Sibudu, South Africa. *Archaeometry*, *60*(5), 1062–1076. https://doi.org/10.1111/arcm.12369

Wragg Sykes, R. M. (2015). To see a world in a hafted tool: Birch pitch composite technology, cognition and memory in Neanderthals. In F. Coward, R. Hosfield, M. Pope, & F. Wenban-Smith

(Eds.), *Settlement, Society and Cognition in Human Evolution* (pp. 117–137). Cambridge University Press. https://doi.org/10.1017/CBO9781139208697.008

Würschem, H., Hoyer, C. T., & Floss, H. (2024). The Châtelperronian Lithic Industries of Eastern France: Germolles and Châtelperron. In H. Koehler, N. J. Conard, & H. Floss (Eds.), *The Rhine During the Middle Paleolithic: Boundary or Corridor?* 315–349.

Yuen, S. N., Choi, S. M., Phillips, D. L., & Ma, C. Y. (2009). Raman and FTIR spectroscopic study of carboxymethylated non-starch polysaccharides. *Food Chemistry*, *114*(3), 1091–1098. https://doi.org/10.1016/j.foodchem.2008.10.053

Zaidner, Y., & Weinstein-Evron, M. (2020). The emergence of the Levallois technology in the levant: A view from the early middle paleolithic site of Misliya Cave, Israel. *Journal of Human Evolution*, *144*, 102785. https://doi.org/10.1016/j.jhevol.2020.102785

Zilhao, J. (2006). Chronostratigraphy of the Middle-to-Upper paleolithic transition in the Iberian Peninsula. *Pyrenae*, 7–84.

Zipkin, A. M., Wagner, M., McGrath, K., Brooks, A. S., & Lucas, P. W. (2014). An experimental study of hafting adhesives and the implications for compound tool technology. *PLoS One*, *9*(11), e112560. https://doi.org/10.1371/journal.pone.0112560

Publisher's Note Springer Nature remains neutral with regard to jurisdictional claims in published maps and institutional affiliations.

Springer Nature or its licensor (e.g. a society or other partner) holds exclusive rights to this article under a publishing agreement with the author(s) or other rightsholder(s); author self-archiving of the accepted manuscript version of this article is solely governed by the terms of such publishing agreement and applicable law.